VILNIUS UNIVERSITY
CENTER FOR PHYSICAL SCIENCES AND TECHNOLOGY

ARNAS DRAZDAUSKAS

EVOLUTIONARY CARBON AND NITROGEN ABUNDANCE ALTERATIONS IN LOW MASS METAL-ABUNDANT STARS

Doctoral Dissertation
Physical Sciences, Physics (02 P)

Vilnius, 2016

Doctoral Dissertation was completed during 2012–2016 at Vilnius University, Institute of Theoretical Physics and Astronomy

Scientific supervisor:

Habil. Dr. Gražina Tautvaišienė (Vilnius University, Physical sciences, Physics – 02 P)

VILNIAUS UNIVERSITETAS
FIZINIŲ IR TECHNOLOGIJOS MOKSLŲ CENTRAS

ARNAS DRAZDAUSKAS

EVOLIUCINIAI ANGLIES IR AZOTO GAUSŲ POKYČIAI MAŽOS MASĖS METALINGOSE ŽVAIGŽDĖSE

Daktaro Disertacija
Fiziniai mokslai, fizika (02 P)

Vilnius, 2016

Daktaro disertacija rengta 2012–2016 metais Vilniaus universiteto Teorinės fizikos ir astronomijos institute

Mokslinė vadovė:

Habil. dr. Gražina Tautvaišienė (Vilniaus universitetas, fiziniai mokslai, fizika – 02 P)

Table of Contents

Introduction

Open star clusters are important in giving us an opportunity to investigate stellar evolution (c.f., Friel et al. 2002; Bragaglia et al. 2008; Jacobson et al. 2009). In open clusters we can analyse a number of stars of essentially the same age, distance, and origin, as stars in such clusters are most likely formed in the same protocloud of gas and dust (see, e.g., Lada & Lada 2003; Pallavicini 2003). Open clusters are physically related multi-object systems of stars bounded together by the gravitational force. Stars inside the open cluster populate a limited region of space, much smaller than their distance from the Sun, so that they are all roughly at the same heliocentric distance. They are believed to originate from large clouds of cosmic gas and dust in the Milky Way. The number of objects in clusters can vary between tenths to thousands of stars.

When having a number of similar targets one can analyse them with higher precision and better statistics, thus their age, distance and other parameters can be determined more precisely than for single field stars. However each star can be treated separately and if chemical abundances in cluster members initially were identical, their changes in stellar atmospheres of evolved stars are mainly related to internal processes of stellar evolution. This circumstance was exploited in a number of studies of open clusters (Gilroy 1989; Gilroy & Brown 1991; Luck 1994; Gonzalez & Wallerstein 2000; Tautvaišienė et al. 2000, 2005; Origlia et al. 2006; Smiljanic et al. 2009; Mikolaitis et al. 2010, 2011a,b, 2012 among others).

Our main goal is to determine abundances of mixing sensitive chemical elements, and carbon and nitrogen in particular. Through CNO cycle, CNO elements play an important role as energy sources in stellar interiors. This affects stellar positions in a Hertzsprung-Russell (HR) diagram and the production of heavy chemical elements. The carbon and nitrogen abundances, C/N, and carbon isotope ratios $^{12}C/^{13}C$ are important tools in studying stellar evolution. When low- and intermediate-mass stars are at the bottom of the giant branch, the first dredge-up takes place (Iben 1965). Surface abundances are further modified when extra-mixing processes be-

come efficient. This happens when low-mass stars reach the luminosity bump on the red giant branch (RGB). Variations of $^{12}C/^{13}C$ and C/N ratios depend on several factors: stellar evolutionary stage, mass, and metallicity (Gilroy 1989; Luck 1994; Gratton et al. 2000; Tautvaišienė et al. 2000, 2005, 2010; Smiljanic et al. 2009, 2016; Mikolaitis et al. 2010, 2011a,b, 2012). On the other hand, exact dependencies are still uncertain (Chanamé et al. 2005; Charbonnel 2006; Cantiello & Langer 2010; Charbonnel & Lagarde 2010; Denissenkov 2010; Lagarde et al. 2011, 2012; Wachlin et al. 2011; Angelou et al. 2012; Lattanzio et al. 2015). There are models which predict different outcomes of mixing effects depending on the stellar turn-off (TO) mass. In this work, we try to fill a lack of observational data and analyse the open clusters with different turn-off masses spanning the wide range of theoretical models, including two young clusters with TO masses $> 5\ M_{\odot}$ that had no previous spectroscopic analyses.

Aims of the study

The main aim of the study is to investigate an influence of the chemical mixing processes in atmospheres of evolved stars. The classical first dredge-up theory cannot account for all observed changes in chemical composition of RGB stars. There have to be some other mechanisms of extra mixing involved, which alter the surface abundances of ^{12}C,^{13}C and ^{14}N beyond the 1^{st} dredge-up model. Most recent models propose thermohaline- and rotation-induced mixing in evolved stars, which depends on mass and metallicity. We aim to determine carbon, nitrogen, and oxygen abundances in red horizontal branch stars of open clusters and compare $^{12}C/^{13}C$ and C/N ratios with most advanced theoretical models.

The second goal is the first high-resolution spectroscopic analysis of stars in two open clusters without such previous analyses and the use of sodium abundance, which is also sensitive to mixing processes, for the evaluation of the theoretical models. We aim to redetermine the main atmospheric parameters for stars in three other open clusters.

Tasks of the study

- Determination of carbon, nitrogen and oxygen abundances as well as C/N and $^{12}C/^{13}C$ ratios in stars of open clusters Collinder 261, Melotte 66, NGC 2324, NGC 2477, NGC 3960, NGC 4609, NGC 5316, NGC 4815, NGC 6705 and Trumpler 20.
- Determination of main atmospheric parameters for red giant stars in the open clusters NGC 4609, NGC 4815, NGC 5316, NGC 6705 and Trumpler 20 and detailed determination of chemical composition in stars of NGC 4609 and NGC 5316
- Comparison of $^{12}C/^{13}C$ and C/N ratios and sodium abundances with theoretical models of evolutionary chemical mixing.

Scientific novelty

Despite the recent increase in studies on mixing processes in evolved stars, there were still too few data points to make definite conclusions on mixing mechanisms acting in stars of different turn-off masses. Our analysis of C/N and $^{12}C/^{13}C$ ratios in ten open clusters adds important data points, especially in the range of larger stellar turn-off masses. Particularly important is the analysis of the C/N and $^{12}C/^{13}C$ ratios in open clusters with turn-off masses larger than four solar masses. Based on the observational data we have evaluated the role of thermohaline- and rotation induced mixing in stars at different turn-off masses.

Among the investigated open clusters there were two (NGC 4609 and NGC 5316) for which there were no high-resolution spectral analyses done before. Their metallicity and detailed chemical composition was determined for the first time using spectral analysis.

Practical importance

Modelling of the mixing processes in stellar interiors can be tested only by acquiring observational data and comparing it with theoretical models. Data from open clus-

ters are best suited for this task due to properties of their member stars and already mentioned precision of analysis and statistics. The observational data of ten new open clusters in the wide range of turn-off masses will be important for developing more precise theoretical models.

Results and statements presented for defence

- The main atmospheric parameters determined for 79 evolved stars in the open clusters NGC 4609, NGC 4815, NGC 5316, NGC 6705, Trumpler 20 and abundances of 11 chemical elements for stars in NGC 4609 and NGC 5316.
- Carbon and nitrogen abundances determined for 109 stars in ten open clusters and oxygen for 68 stars in nine open clusters, $^{12}C/^{13}C$ ratios in 27 evolved stars of seven open clusters and C/N ratios for 109 stars in 10 open clusters.
- The average values of $^{12}C/^{13}C$ ratios in He-core burning stars in our sample of open clusters with turn-off masses lower than 1.5 $M_{\odot}$ agree well with the thermohaline-induced mixing as well as with the model where thermohaline- and rotation-induced mixing act together. For turn-off masses larger than 2 $M_{\odot}$, the mean values of $^{12}C/^{13}C$ agree well with the model of pure thermohaline-induced mixing or the first dredge-up model. They are not lowered as much as predicted by the thermohaline- and rotation-induced mixing model.
- The mean C/N values for open clusters in our study with turn-off masses lower than about 3 $M_{\odot}$ agree well with the model of both the pure thermohaline-induced extra-mixing and the first dredge-up. For turn-off masses $\geq 5M_{\odot}$ the C/N ratios agree with the thermohaline- and rotation-induced mixing model, however, the results also agree within errors with the first dredge-up model.
- The $^{12}C/^{13}C$ and C/N ratios in the investigated clump stars of NGC 3960 (turn-off mass is about 2 $M_{\odot}$) are not homogeneous. This cluster probably contains stars which are affected by the pure thermohaline-induced mixing or the first dredge-up as well as stars which are influenced by rotation-induced mixing or other extra-mixing mechanisms.

Personal contribution

All the work related to the determination of the main atmospheric parameters of stars and chemical composition study was done by the author. The author interpreted the chemical composition results and drew conclusions together with the co-authors of the study.

Publications on the subject of the dissertation

1. Cantat-Gaudin T., Vallenari A., Zaggia S., Bragaglia A., Sordo R., Drew J. E., Eisloeffel J., Farnhill H. J., Gonzalez-Solares E., Greimel R., Irwin M. J., Kupcu-Yoldas A., Jordi C., Blomme R., Sampedro L., Costado M. T., Alfaro E., Smiljanic R., Magrini L., Donati P., Friel E. D., Jacobson H., Abbas U., Hatzidimitriou D., Spagna A., Vecchiato A., Balaguer-Nunez L., Lardo C., Tosi M., Pancino E., Klutsch A., Tautvaišienė G., **Drazdauskas A.**, Puzeras E., Jiménez-Esteban F., Maiorca E., Geisler D., San Roman I., Villanova S., Gilmore G., Randich S., Bensby T., Flaccomio E., Lanzafame A., Recio-Blanco A., Damiani F., Hourihane A., Jofré P., de Laverny P., Masseron T., Morbidelli L., Prisinzano L., Sacco G. G., Sbordone L., Worley C. C., *The Gaia-ESO Survey: Stellar content and elemental abundances in the massive cluster NGC 6705*, Astronomy & Astrophysics, Vol. 569, A17, 18 pp, 2014.

2. Tautvaišienė G., **Drazdauskas A.**, Mikolaitis Š., Barisevičius G., Puzeras E., Stonkutė E., Chorniy Y., Magrini L., Romano D., Smiljanic R., Bragaglia A., Carraro G., Friel E., Morel T., Pancino E., Donati P., Jiménez-Esteban F., Gilmore G., Randich S., Jeffries R. D., Vallenari A., Bensby T., Flaccomio E., Recio-Blanco A., Costado M. T., Hill V., Jofré P., Lardo C., de Laverny P., Masseron T., Moribelli L., Sousa S. G., Zaggia S., *The Gaia-ESO Survey: CNO abundances in the open clusters Trumpler 20, NGC 4815, and NGC 6705*, Astronomy & Astrophysics, Vol. 573, A55, 2015.

3. **Drazdauskas A.**, Tautvaišienė G., Randich S., Bragaglia A., Mikolaitis Š., and Janulis R., *The extent of mixing in stellar interiors: the open clusters Collinder 261 and Melotte 66*, Astronomy & Astrophysics, Vol. 589, A50,

2016.

4. Tautvaišienė G., Smiljanic R., Bagdonas V., **Drazdauskas A.**, Mikolaitis Š., *The role of asymptotic giant branch stars in the chemical evolution of the Galaxy*, Memorie della Societa Astronomica Italiana, Vol. 87, p.315, 2016.

5. **Drazdauskas A.**, Tautvaišienė G., Smiljanic R., Bagdonas V., Chorniy Y., *Chemical composition of evolved stars in the young open clusters NGC 4609 and NGC 5316*, Monthly Notices of the Royal Astronomical Society, Vol. 462, Issue 1, p.794-803, 2016.

6. Tautvaišienė G., **Drazdauskas A.**, Bragaglia A., Randich S., Ženovienė R., 2016, *C, N, O abundances and carbon isotope ratios in evolved stars of the open clusters NGC 2324, NGC 2477, and NGC 3960*, Astronomy & Astrophysics, Vol. 595, A16, 2016.

7. **Drazdauskas A.**, Tautvaišienė G., Mikolaitis Š., Barisevičius G., Puzeras E., Stonkutė E., Chorniy Y., and GES colaborators, *The Gaia-ESO Survey: CNO abundances in open clusters of our Galaxy*, 2016, Astronomical Society of the Pacific Conference Series, in press.

Presentations at international conferences

1. Tautvaišienė G., **Drazdauskas A.**, Mikolaitis Š., Barisevičius G., Chorniy Y., Puzeras E., Smiljanic R., Sestito P., Geisler D., Villanova S., San Roman I., *CNO abundances in open clusters*, "Gaia-ESO Survey First Science meeting", 2013, Nice (France), 8-11 April, 2013 (Poster presentation by G. Tautvaišienė).

2. Tautvaišienė G., **Drazdauskas A.**, Stonkutė E., Mikolaitis Š., Barisevičius G., Puzeras E., Chorniy Y. and the Gaia-ESO survey consortium, *The Gaia-ESO Survey: CNO abundances in Galactic Open clusters and Field Stars*, European Astronomical Society symposium "Gaia Research for European Astronomy Training: GREAT network science, European Week of Astronomy and Space Science, Geneva (Switzerland), 30 June - 4 July, 2014 (Poster presentation by G. Tautvaišienė).

3. **Drazdauskas A.**, Tautvaišienė G., Mikolaitis Š., Barisevičius G., Puzeras E., Stonkutė E., Chorniy Y., and GES colaborators, *The Gaia-ESO Survey: CNO abundances in open clusters of our Galaxy*, International conference "Multi-Object Spectroscopy in the Next Decade: Big Questions, Large Surveys and Wide Fields", Santa Cruz de La Palma (Spain), 2-6 March, 2015 (Poster presentation).

4. **Drazdauskas A.**, Tautvaišienė G., Randich S., Mikolaitis Š., *Cheminio maišymosi procesų tyrimas mažos masės padrikųjų spiečių žvaigždėse*, "41-oji Lietuvos Nacionalinė Fizikos Konferencija", Vilnius (Lithuania), 17-19 June, 2015 (Poster presentation).

5. Bagdonas V., Tautvaišienė G., Smiljanic R., **Drazdauskas A.**, Mikolaitis Š., *Sunkiųjų cheminių elementų gausa padrikųjų spiečių raudonosiose milžinėse*, "41-oji Lietuvos Nacionalinė Fizikos Konferencija", Vilnius (Lithuania), 17-19 June, 2015 (Poster presentation by V. Bagdonas).

6. Tautvaišienė G., Smiljanic R., Bagdonas V.,**Drazdauskas A.**, Mikolaitis Š., Magrini L., *The role of asymptotic giant branch stars in the chemical evolution of the Galaxy*, European Astronomical Society special session "AGB stars: a key ingredient in the understanding and interpretation of stellar populations", European Week of Astronomy and Space Science, La Laguna, Tenerife, (Spain), 22-26 June, 2015 (Poster presentation by L. Magrini).

7. Tautvaišienė G., Mikolaitis Š., Kordopatis G., Stonkutė E., **Drazdauskas A.**, Smiljanic R., Valentini M., Puzeras E., Magrini L., and Gaia-ESO Consortium, *The Gaia-ESO Survey: CNO and alpha-element distributions in the Galactic discs*, European Astronomical Society special session "Chemical abundances and gradients in spatially resolved late-type Galaxies in the Local Universe", European Week of Astronomy and Space Science, La Laguna, Tenerife, (Spain), 22-26 June, 2015 (Poster presentation by L. Magrini).

8. Tautvaišienė G., **Drazdauskas A.**, Randich S., Smiljanic R., Mikolaitis Š., *Diagnostics of mixing processes in atmospheres of low-mass stars*, IAU Symposium "Stellar Physics in Galaxies Throughout the Universe", XXIX (29th) In-

ternational Astronomical Union General Assembly, Honolulu, Hawaii (USA), 3-14 August, 2015 (Poster presentation by G. Tautvaišienė).

9. Tautvaišienė G., **Drazdauskas A.**, Lardo C., Martell S. L., Pancino E., Stonkutė E., & Gaia-ESO Consortium, *The Gaia-ESO Spectroscopic Survey: CNO abundances ingiants of the multiple-population globular cluster NGC 1851*, IAU Symposium "The General Assembly of Galaxy Halos: Structure", Origin and Evolution", XXIX (29th) International Astronomical Union General Assembly, Honolulu, Hawaii (USA), 3-14 August, 2015 (Poster presentation by G. Tautvaišienė).

10. **Drazdauskas A.**, Smiljanic R., Tautvaišienė G. and Bagdonas V., *CNO abundances in low mass stars of open clusters*, "Gaia-ESO Survey Third Science Meeting", Vilnius (Lithuania), 1-4 December, 2015 (Poster presentation).

11. Ženovienė R., Tautvaišienė G., **Drazdauskas A.**, Mikolaitis Š., *Carbon to nitrogen ratio in stars of open clusters*, COST Action international conference "Origins and evolution of Life in the Universe, From Star and Planet Formation to Early Life", Vilnius (Lithuania), 25-28 April, 2016 (Poster presentation by R. Ženovienė).

12. **Drazdauskas A.**, Bagdonas V., Randich S., Bragaglia A., Smiljanic R., Tautvaišienė G., *Carbon, Nitrogen and Oxygen abundances in evolved low mass stars of open clusters*, COST Action international conference "Origins and evolution of Life in the Universe, From Star and Planet Formation to Early Life", Vilnius (Lithuania), 25-28 April, 2016 (Poster presentation).

Thesis outline

The work consists of following parts: Introduction, four main chapters and references.

Chapter 1 presents the summary of data on target clusters.

Chapter 2 consists of information about differential analysis methods, stellar models and software packages used for determination of results, as well as uncertainties encountered during the work process.

Chapter 3 provides all obtained results, their comparison with theoretical models and results determined in other studies.

Chapter 4 is dedicated to the summary of results and conclusions.

Chapter 1

1.1 Cluster data

The target clusters were selected from a few ongoing projects. The most important one is the Gaia-ESO public spectroscopic survey (GES) which targets over 10^5 stars in the Milky Way. The main goal of this project is to provide the first truly homogeneous overview of the kinematics and chemical abundances in our Galaxy. The survey targets not only open and globular clusters, but stars in different regions in the Galaxy, including the Bulge, the Halo and different star forming regions. This will help to significantly advance the research of stellar and Galactic evolution.

The other important project is the Bologna Open Clusters Chemical Evolution project (BOCCE). One of the main goals of this survey is to improve our understanding of mixing processes in stars and their chemical abundance gradients according to the galactocentric distance. To achieve this, the project chose about 30 open clusters evenly distributed in the age, metallicity and galactocentric distances. During the course of the project, age, metallicity, distance, reddening and chemical element abundances will be derived homogeneously, to allow for the accurate determination of possible trends.

And the third one is a collaborative project run with our colleague R. Smiljanic, who has observed a number of young clusters. Some of them had no previous spectroscopic studies at all, some were partially analysed, however, mixing processes will be analysed for the first time for almost all of them. The parameters of target stars are presented in Table 1.1.

We have chosen to analyse only RGB and red clump stars in the target clusters selected according to their photometric data because our main interest lies in the mixing processes in evolved stars. The main reason being that only when a star enters the RGB phase, the changes in its chemical abundance become apparent.

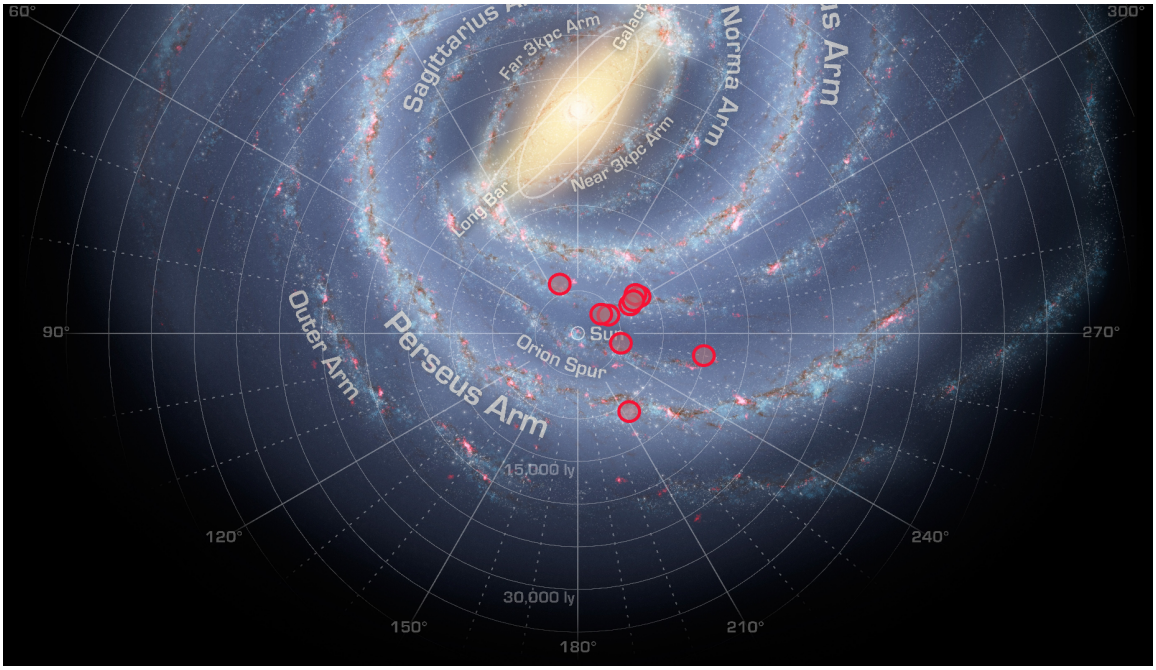

Figure 1.1: Positions of our target open clusters in the Galaxy marked as red circles. Image credit: NASA/JPL-Caltech/R. Hurt.

1.2 Cluster parameters

1.2.1 Collinder 261

The first target cluster in our work is the open cluster Collinder 261 (Cr 261). This cluster is located at galactic coordinates $l = 301°.68$, $b = -5°.53$. The first survey of the open cluster Cr 261 was made by van den Bergh & Hagen (1975). They determined it was a rich cluster with a diameter of 8 arcmin. Phelps et al. (1994) provided the first CCD photometry and claimed Cr 261 was one of the oldest clusters, although no precise age was given. A very old age was confirmed by later studies (Mazur et al. 1995 suggested 5 Gyr, Gozzoli et al. 1996 gave a range of 7 – 11 Gyr, and Bragaglia & Tosi 2006 preferred an age of 6 Gyr). The low-resolution spectroscopic study by Friel (1995) determined a metallicity [Fe/H]=-0.14 which was updated to [Fe/H]=-0.15 ± 0.13 by Friel et al. (2002), based on 21 stars. Friel et al. (2003) analyse four stars with high resolution spectroscopy and determine [Fe/H]=-0.22 ± 0.05. The following high-resolution spectroscopic studies determine a slightly higher metal content. Carretta et al. (2005) investigate six red clump and RGB stars and find [Fe/H]=-0.03 ± 0.03 for the five warmer stars. De Silva

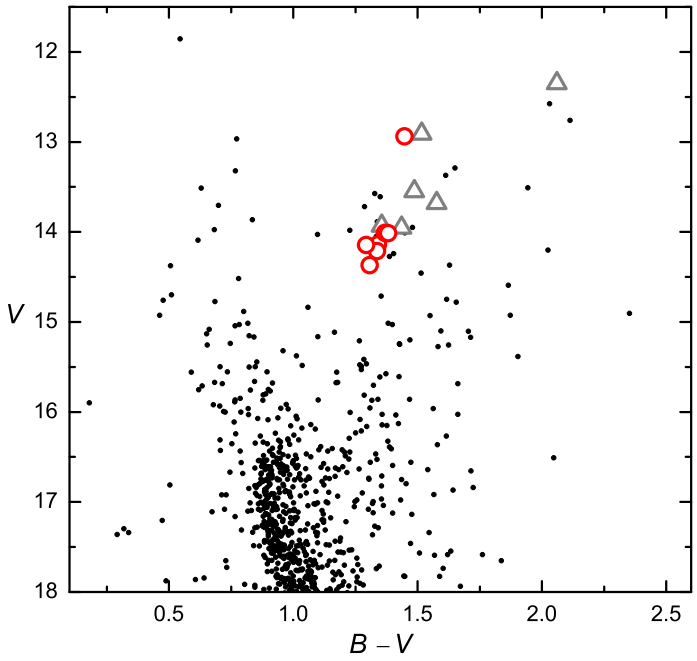

Figure 1.2: Colour-magnitude diagram of the open cluster Collinder 261. The stars investigated in this work are indicated by circles, while the stars of Mikolaitis et al. (2012) are indicated with open triangles. The diagram is based on BVI photometry by Gozzoli et al. (1996).

et al. (2007) also determine [Fe/H]=-0.03 ± 0.05. Sestito et al. (2008) obtained spectra with two UVES setups (see later), but base their results mostly on the bluer ones. They determine [Fe/H]= 0.13 ± 0.05 for seven RGB and red clump stars. We use the spectra of both their setups.

The only study of CNO elements and carbon isotope ratios in Collinder 261 was performed by Mikolaitis et al. (2012). Using high resolution FEROS spectra of the six stars previously investigated by Carretta et al. (2005), they determine a mean carbon-to-nitrogen ratio of $1,67 \pm 0,06$. The average value of $^{12}C/^{13}C$=18 ± 2 was determined in four giants, and 12 ± 1 in two clump stars. Their results agree with the theoretical cool bottom processing model proposed by Boothroyd & Sackmann (1999) and with the thermohaline-induced mixing model computed by Charbonnel & Lagarde (2010).

1.2.2 Melotte 66

The first mention of Melotte 66 (Mel 66; galactic coordinates $l = 259^\circ.56$, $b = -14^\circ.24$) can be found in the work by Eggen & Stoy (1962). They performed a photographic BV photometry for 20 stars. King (1964) made a suggestion that this cluster is one of the oldest in our Galaxy. Various authors quote rather similar ages, ranging from 4 to 7 Gyr (Hawarden 1976; Anthony-Twarog et al. 1979; Gratton 1982; Friel & Janes 1993; Kassis et al. 1997). In the present work we assume the age of Kassis et al. (1997), i.e. 4 Gyr.

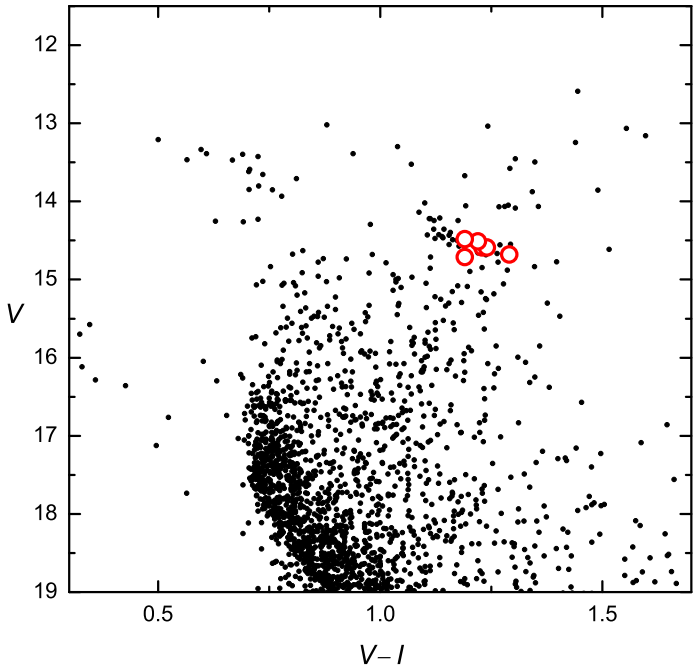

Figure 1.3: Colour-magnitude diagram of the open cluster Melotte 66. The stars investigated in this work are indicated by circles. The diagram is based on VIc CCD photometry by Kassis et al. (1997).

The photometric analyses of Melotte 66 consistently provide low values for its metallicity, about -0.5 dex (Hawarden 1976; Dawson 1978; Geisler & Smith 1984; Twarog et al. 1995). This was confirmed by moderate-resolution (Friel & Janes 1993 determined [Fe/H]=-0.51 ± 0.11 from four giants) and by high-resolution spectroscopy (Gratton & Contarini 1994 determined [Fe/H]=-0.38 ± 0.15 from two giants). The most recent investigation was carried out by Sestito et al. (2008) using high-resolution spectra of six giants with mean [Fe/H]=-0.33 ± 0.03.

There are no previous investigations of CNO abundances or $^{12}C/^{13}C$ ratios for this cluster. In particular, we use the spectra of the five stars that are considered members and are not fast rotators.

1.2.3 NGC 2324

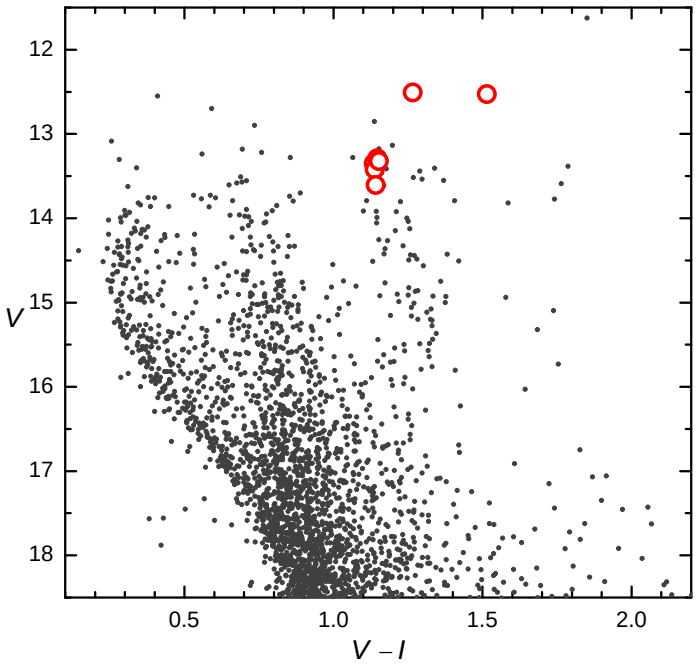

Figure 1.4: Colour-magnitude diagram of the open cluster NGC 2324. The stars investigated in this work are indicated by circles. The diagram is based on *VIc* photometry by Kyeong et al. (2001).

Investigations of NGC 2324 (galactic coordinates $l = 213°.45$, $b = +03°.30$) have begun with Cuffey (1941), who built a colour-magnitude diagram and estimated a distance of about 3320 parsecs. NGC 2324 is a relatively young cluster. Kyeong et al. (2001) determined an age of about 630 Myr, a Galactocentric distance $R_{gc} =$ 11.7 kpc, and [Fe/H]~ -0.32 using *UBVIc* CCD photometry and isochrone fitting. More recently, Piatti et al. (2004) used *VIc* and *Washington* photometry to derive an age of about 440 Myr, a distance of 3.8 kpc, reddening 0.25 mag, and metallicity of about -0.30 dex. The analysis of low-resolution spectra reported by Friel et al. (2002) provided [Fe/H]$=-0.15 \pm 0.16$, while the analysis of high-resolution spectra, which we use here, has been performed by Bragaglia et al. (2008) and produced [Fe/H]$=-0.17 \pm 0.05$.

1.2.4 NGC 2477

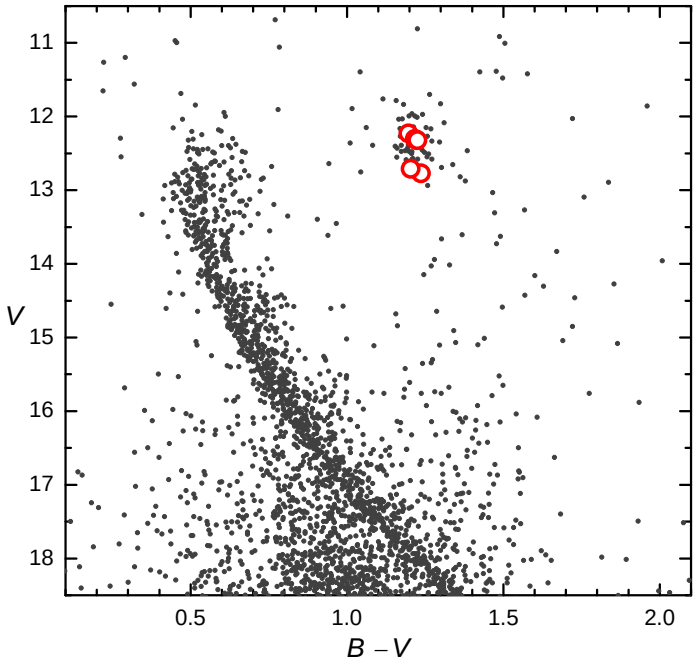

Figure 1.5: Colour-magnitude diagram of the open cluster NGC 2447. The stars investigated in this work are indicated by circles. The diagram is based on *UBV* photometry by Kassis et al. (1997).

Photometry of NGC 2477 (located at $l = 253^\circ.56$, $b = -05^\circ.84$) was first made by Eggen & Stoy (1961). Hartwick et al. (1972) suggested based on further photometric observations that the metallicity of NGC 2477 is approximately 1.5 times that of the Hyades and the age is about 1.5 Gyr. Kassis et al. (1997) used deep *UBVI* photometry and isochrone fitting (with $[\mathrm{Fe/H}] = -0.05 \pm 0.11$ from Friel & Janes (1993) and reddening 0.2–0.4 mag from Hartwick et al. (1972) to derive an age of about 1 Gyr and $R_{\mathrm{gc}} = 8.94$ kpc. Kharchenko et al. (2013) reported an approximate distance from the Sun of 1.5 kpc for this cluster and an age equal to 820 Myr. The low-resolution spectroscopy performed by Friel et al. (2002) gave $[\mathrm{Fe/H}] = -0.13 \pm 0.10$. The high-resolution spectroscopic metallicity value is $[\mathrm{Fe/H}] = 0.07 \pm 0.03$ (Bragaglia et al. 2008).

1.2.5 NGC 3960

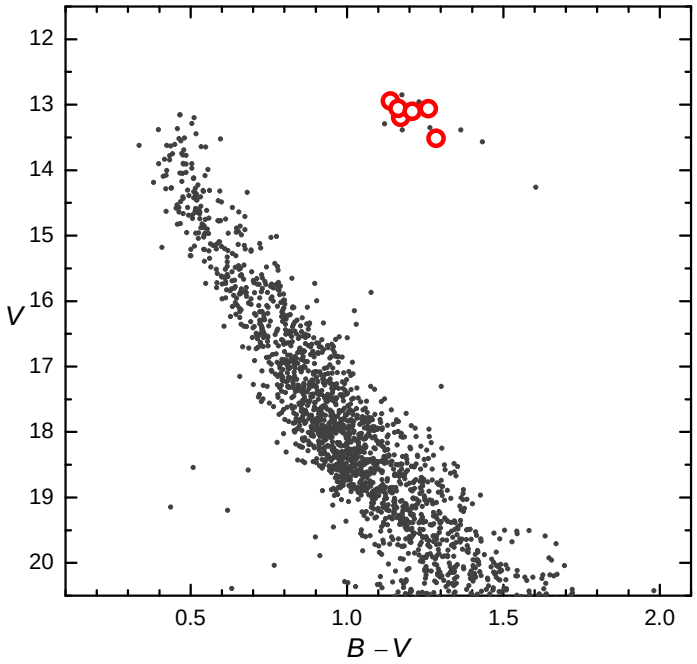

Figure 1.6: Colour-magnitude diagram of the open cluster NGC 3960. The stars investigated in this work are indicated by circles. The diagram is based on *UBV* photometry by Bragaglia et al. (2006).

NGC 3960 (galactic coordinates $l = 294°.37$, $b = +06°.18$) was identified by van den Bergh & Hagen (1975). Its first colour-magnitude diagram was built by Janes (1981). Prisinzano et al. (2004) investigated this cluster using *BVI* filters and determined its age as between 0.9 and 1.4 Gyr. Bragaglia et al. (2006) presented *UBVI* photometry and derived an age of 0.6 to 0.9 Gyr from a comparison of observed and synthetic CMDs, using tracks without and with overshooting, respectively. The higher value is to be preferred; the corresponding distance modulus and reddening place the cluster at R_{gc}=7.4 kpc and z=220 pc above the Galactic plane. The metallicity of the cluster has been studied extensively. The photometric metallicity determinations range from $[Fe/H] = -0.68$ (determined by Geisler et al. 1992 using Washington photometry) to -0.06 dex by Piatti et al. 1998, who used *DDO* photometry. Based on low-resolution spectra, Friel & Janes (1993) determined $[Fe/H] = -0.34$, and Twarog et al. (1997) determined $[Fe/H] = -0.17$. A high-resolution spectral analysis of three stars by Bragaglia et al. (2006) resulted in $[Fe/H] = -0.12 \pm 0.04$, and Sestito et al. (2006) derived the mean value as

[Fe/H] $= +0.02 \pm 0.04$ from the higher signal-to-noise ratio spectra of six stars.

1.2.6 NGC 4609

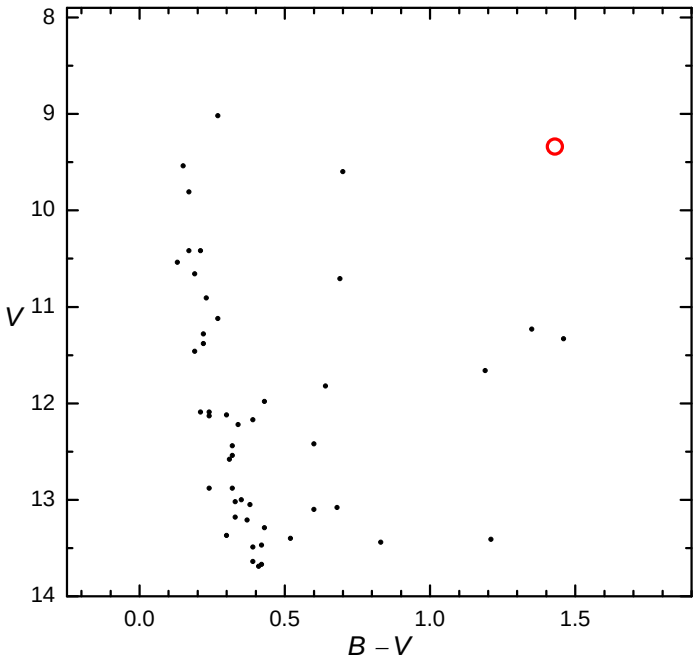

Figure 1.7: The colour-magnitude diagram of the open cluster NGC 4609. The star investigated in this work is indicated by the circle. The diagram is based on UBV photometry by Feinstein & Marraco (1971).

NGC 4609 is located towards galactic center at $l = 301^{\circ}.89$, $b = -00^{\circ}.14$. There are few previous photometric studies and no spectroscopic ones for this cluster. The first ever study of NGC 4609 was by Feinstein & Marraco (1971). Their photoelectric UBV observations and analysis of the cluster provided the age of 60 Myr and the distance of 1320 pc as well as identified 33 sure members. Consecutive age determinations range from 36 Myr (Battinelli & Capuzzo-Dolcetta 1991) to 125 Myr (Kharchenko et al. 2013). van den Bergh & Hagen (1975) verified, that this cluster is indeed a very poor one. The following photometric studies confirmed the distance (Mermilliod 1981) and poor membership (Janes & Adler 1982). Jura (1987) made a rough estimate of TO mass to be around 7 $M_{\odot}$.

The only metallicity determination was made by Claria et al. (1989). They obtained UBV, DDO and Washington photometry for G and K stars and found a metallicity of about 0.05 ± 0.13.

1.2.7 NGC 4815

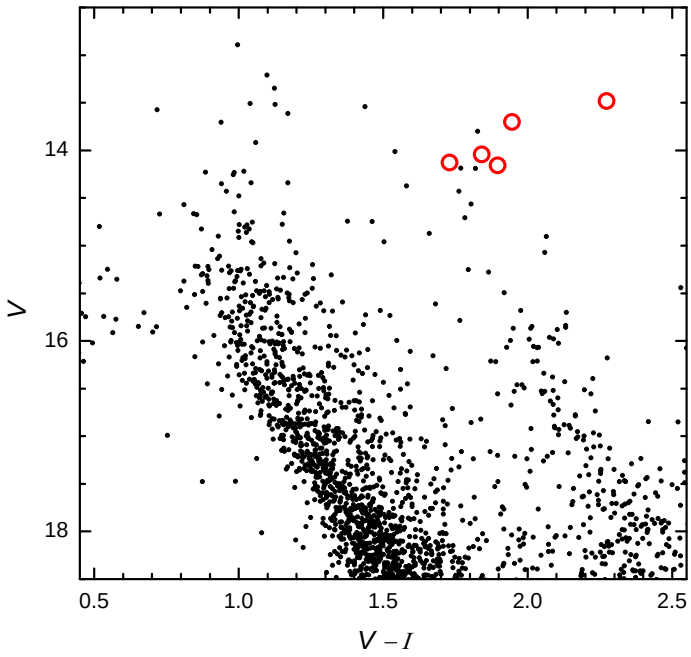

Figure 1.8: Colour-magnitude diagram of the open cluster NGC 4815. The stars investigated in this work are indicated by circles. The diagram is based on photometry by Prisinzano et al. (2001).

NGC 4815 is a intermediate age cluster toward the centre of the Galaxy with galactic coordinates $l = 303^{\circ}.63,\ b = -02^{\circ}.10$. The first study of this cluster was by Moffat & Vogt (1973). Using photoelectric $UBV - \mathrm{H}\beta$ photometry they made a conclusion that NGC 4815 probably is not a cluster. However the following study by van den Bergh & Hagen (1975), contrary to the Moffat & Vogt, confirmed that this is in fact a rich open cluster. There has been more than a few following photometric studies for NGC 4815. Kjeldsen & Frandsen (1991) using UBV photometry determined that the distance to the cluster is $\sim$2.8 kpc and by fitting theoretical isochrones they derived the age of about 200 Myrs. The study by Carraro & Ortolani (1994) obtained BVCCD photometry and derived a probable age of 500 Myrs, distance of arounf 2.5 kpc, and by fitting isochrones of different metallicities they came to a conclusion, that the cluster most probably has a lower than solar [Fe/H] content which is about -0.40. The most recent photometric study was by Prisinzano et al. (2001), who obtained BVI photometry and determined the age of 400 Myrs, distance of about 2.75 kpc and the metallicity content of around or slightly above solar.

NGC 4815 has not been observed spectroscopically before GES. According to GES data, a mean [Fe/H] was determined to be equal to $+0.03 \pm 0.05$ dex. Comparisons with three different sets of isochrones yielded consistent determinations of the cluster age of 0.5 to 0.63 Gyr, a turn-off mass of 2.6 ± 0.1 a distance of 2.5–2.7 kpc, and R_{GC}=6,9 kpc (Friel et al. 2014).

1.2.8 NGC 5316

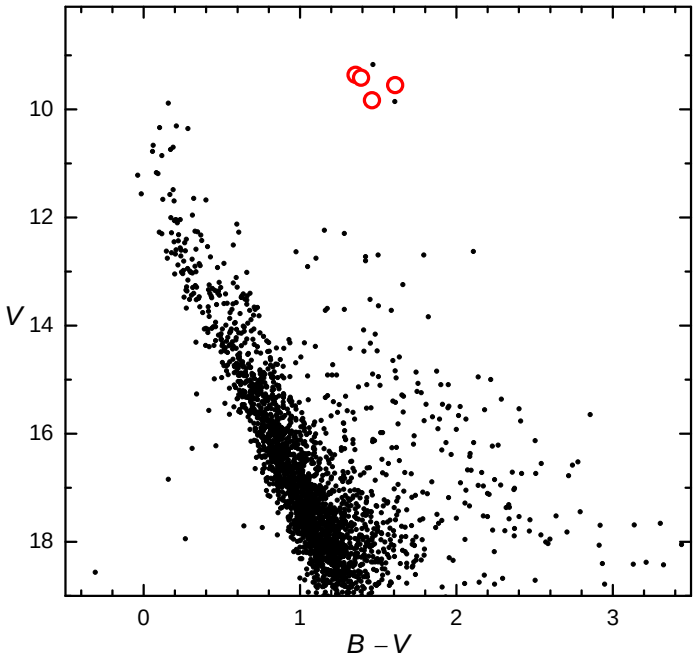

Figure 1.9: The colour-magnitude diagram of the open cluster NGC 5316. The stars investigated in this work are indicated by circles. The diagram and the three red stars are based on *UBV* CCD photometry by Carraro & Seleznev (2012) and the star marked by empty red circle is from T. Oja (private communication).

NGC 5316 is a very young open cluster located at $l = 310°.23$, $b = 00°.12$. The first photometric age and distance determination was made by Lindoff (1968). They derive the age to be 51 Myr and the distance around 1.12 kpc. The following photometric analysis of the cluster provided similar distance values, ranging from 1.08 kpc (Becker & Fenkart 1971) to 2 kpc (Chen et al. 2003). The determined galactocentric distances do not vary by much as well (from 7.4 by Chen et al. (2003) to 7.745 by Hou et al. (2002) Age determinations, however, vary more significantly from the already mentioned determination by Lindoff (1968) to around 195 Myr by Battinelli

& Capuzzo-Dolcetta (1991). The most recent determination of about 170 Myr coming from Kharchenko et al. (2013). The newest study by Carraro & Seleznev (2012) using UBVI CCD photometry provide the age of 100 Myr, distance of 1.4 kpc and Rgc of 7.6 kpc, as well as values for reddening $E(B-V) = 0.25 \pm 0.05$ mag and distance modulus $(m-M) = 11.50 \pm 0.2$ mag. The only TO mass determination was made by Jura (1987), who provides a value of about 4 $M_{\odot}$.

This cluster has numerous photometric metallicity determinations. The first one being by Claria et al. (1989) who used multiple photometric systems to derive $[\mathrm{Fe/H}] = 0.19 \pm 0.11$ from 7 RGB stars. The few following studies by Piatti et al. (1995) and Twarog et al. (1997) used the same *DDO* photometry as Claria et al. (1989), however, different analysis methods were applied. The resulting derived abundances were $[\mathrm{Fe/H}] = -0.02 \pm 0.12$ and $[\mathrm{Fe/H}] = 0.128 \pm 0.127$, respectively. The newest study by Kharchenko et al. (2013) provide the metallicity content of $[\mathrm{Fe/H}] = 0.045$

1.2.9 NGC 6705

NGC 6705 is probably the most extensively studied open cluster. It is included in the ongoing Gaia-ESO public spectroscopic survey and is being analysed in scrutiny. It is a massive and concentrated OC located in the first galactic quadrant (Messina et al. 2010; Santos et al. 2005) at the galactic coordinates $l = 27^{\circ}.31,\ b = -2^{\circ}.80$. This cluster contains a total of several thousand solar masses (McNamara et al. 1977; Santos et al. 2005), which places it near the limit between the most massive OCs and the least massive GCs (Bragaglia et al. 2012). The first mention of this cluster was over a hundred and fifty years ago by Messier, hence the alternative name of the cluster - Messier11. The first photometry, however, came a hundred years later by Johnson et al. (1956). They derived the distance of 1.66 kpc. The more recent photometric studies by Sung et al. (1999); Santos et al. (2005); Koo et al. (2007) provide roughly the same age estimate of about 220-250 Myrs.

There has been more than a few spectroscopic studies, which mainly included the estimation of radial velocity for the cluster (Mermilliod et al. 2008; Frinchaboy & Majewski 2008; Mathieu et al. 1986). Gonzalez & Wallerstein (2000) determined metallicity value of [Fe/H]=0.10, which was followed by the work by Heiter et al.

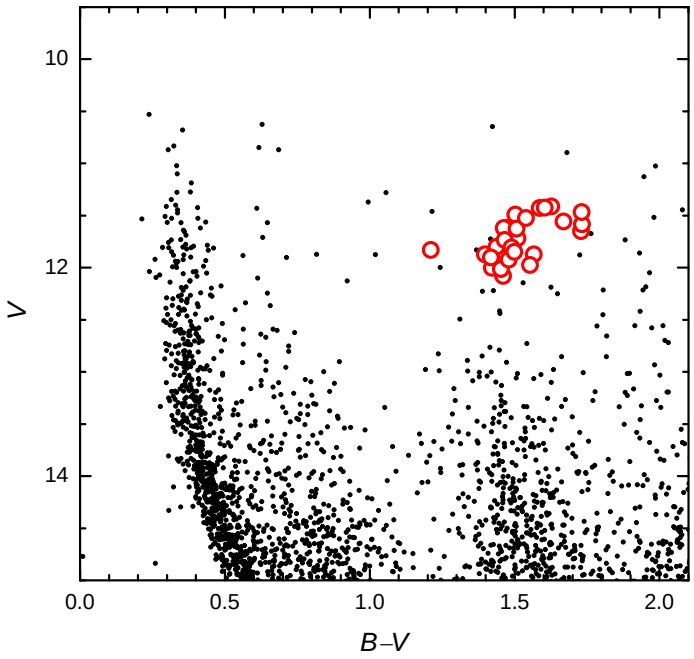

Figure 1.10: Colour-magnitude diagram of the open cluster NGC 6705. The stars investigated in this work are indicated by circles. The diagram is based on photometry by Sung et al. (1999).

(2014) who derived [Fe/H]=0.12. As determined by the most extensive study by Cantat-Gaudin et al. (2014) on the basis of GES data, the age of NGC 6705 is in the range from 0.25 to 0.32 Gyr, the turn-off mass from 3.47 to 3.2 M, depending on the adopted stellar model, and the Galactocentric radius is equal to 6.3 kpc. The average iron abundance of 21 members was [Fe/H]=0.10 ± 0.06.

1.2.10 Trumpler 20

Trumpler 20 is located at $l = 301^{\circ}.50$, $b = +2^{\circ}.20$ and was identified by van den Bergh & Hagen (1975) as being a rich open cluster. It is a relatively old open cluster which does not have many studies until recently. McSwain & Gies (2005) performed only the second study for this cluster. They searched for B and Be stars. However they apparently made a mistake when fitting the CMD with isochrone, which resulted in age determination of only 160 Myrs which is greatly underestimated. The following study by Platais et al. (2008) using BVI photometry and fitting of Padova isochrones provided an age of 1.3 Gyrs and a slightly subsolar metallicity. They used the FEROS spectrograph to observe 6 red giant stars in this cluster, 5 of

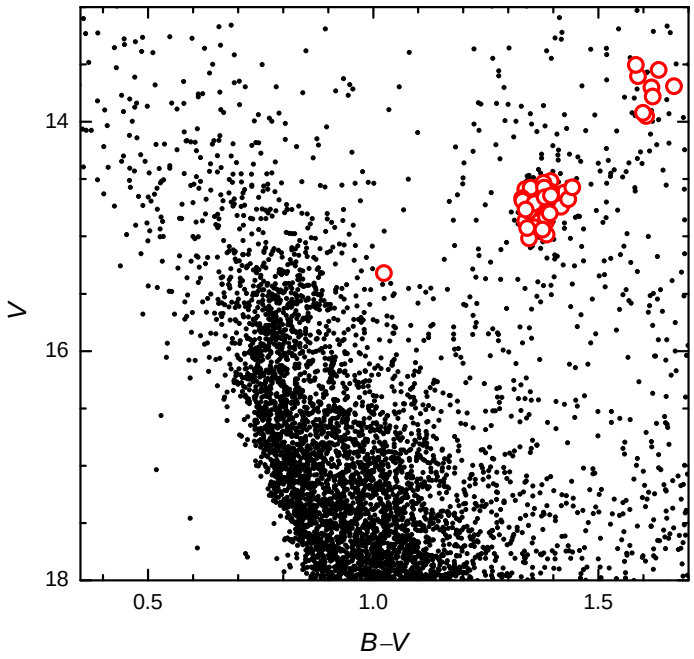

Figure 1.11: Colour-magnitude diagram of the open cluster Trumpler 20. The stars investigated in this work are indicated by circles. The diagram is based on photometry by Carraro et al. (2010).

which turned out to be members based on radial velocity. Out of those five, one had a sufficient S/N ratio for spectroscopic analysis which yielded a $[\mathrm{Fe/H}] = -0.11$. Seleznev et al. (2010) used VI photometry and derived cluster age of around 1.5 Gyrs and R_{gc}=7.3 kpc by fitting Padova isochrones of solar metallicity. 1.4 Gyrs was determined by Carraro et al. (2010) as well using Padova isochrones and their own UBVI photometry. A global survey performed by Kharchenko et al. (2013) provides the age of 2.1 Gyrs and metallicity of -0.11 ± 0.13.

Based on the first internal GES data release and photometric observations, comparisons with three different sets of isochrones yielded consistent determinations of the cluster age of 1.35 to 1.66 Gyr, a turn-off mass of $1.9 \pm 0.1\ M_{\odot}$, a distance of 3.4–3.5 kpc, the Galactocentric radius of 6.88 kpc, and the average iron abundance of 13 members was [Fe/H]=0.17 (Donati et al. 2014). However almost at the same time another parallel study was performed by Carraro et al. (2014). Based on their own observed spectra of sample of red giant stars they derived $[\mathrm{Fe/H}] = 0.09 \pm 0.10$.

Table 1.1: Parameters for stars in target clusters

ID	l	b	V	$B-V$	$V-I$	RV	S/N
	deg (J2000)	deg (J2000)	mag	mag	mag	km s^{-1}	
			Trumpler 20				
2730	189.6498	–60.7568	14.942	1.376		–41.39	33
2690	189.6525	–60.7583	14.572	1.442		–42.57	20
63	189.7420	–60.5079	13.603	1.588		–42.35	71
292	189.7671	–60.5667	13.506	1.583		–40.45	72
1082	189.7699	–60.6965	14.800	1.392		–41.78	36
724	189.7796	–60.6349	15.018	1.346		–41.44	31
794	189.7918	–60.6445	13.703	1.618		–41.89	57
582	189.7964	–60.6146	14.923	1.358		–42.66	36
542	189.8000	–60.6089	14.690	1.332		–41.80	40
340	189.8157	–60.5779	14.669	1.331		–40.01	36
770	189.8577	–60.6411	14.928	1.342		–42.60	23
950	189.8599	–60.6727	14.831	1.384		–41.85	27
505	189.8625	–60.6015	14.519	1.394		–40.02	46
894	189.8805	–60.6617	14.766	1.339		–36.09	40
203	189.9059	–60.5491	14.865	1.338		–41.44	29
835	189.9076	–60.6514	14.577	1.380		–40.69	32
1010	189.9188	–60.6835	14.643	1.395		–42.79	32
923	189.9218	–60.6678	14.872	1.384		–39.32	37
858	189.9295	–60.6554	14.676	1.433		–41.82	31
227	189.9328	–60.5546	14.590	1.338		–41.00	33
346	189.9341	–60.5781	14.704	1.366		–41.08	35
781	189.9365	–60.6428	14.610	1.395		–39.37	36
768	189.9382	–60.6405	14.789	1.380		–41.50	38
791	189.9415	–60.6441	14.535	1.378		–39.72	44
287	189.9454	–60.5650	14.781	1.346		–40.99	37
1008	189.9465	–60.6829	13.949	1.606		–40.30	54
795	189.9476	–60.6448	14.712	1.358		–40.00	32
246	189.9541	–60.5578	14.575	1.350		–39.67	30

Table 1.1 – continued from previous page

ID	l	b	V	$B-V$	$V-I$	RV	S/N
	deg (J2000)	deg (J2000)	mag	mag	mag	km s^{-1}	
787	189.9761	–60.6436	14.597	1.385		–42.45	45
638	189.9815	–60.6241	14.613	1.381		–41.06	57
430	189.9820	–60.5898	15.322	1.024		–38.99	25
827	189.9856	–60.6503	14.805	1.384		–38.99	39
885	189.9880	–60.6593	14.660	1.381		–42.06	42
399	189.9990	–60.5853	14.618	1.425		–42.10	53
129	190.0046	–60.5276	14.716	1.420		–40.90	39
429	190.0048	–60.5894	14.615	1.393		–40.87	43
911	190.0108	–60.6651	13.780	1.621		–41.29	72
1044	190.0116	–60.6887	14.985	1.385		–39.09	27
591	190.0188	–60.6157	13.690	1.668		–41.65	62
468	190.0315	–60.5957	13.548	1.634		–41.12	60
679	190.0929	–60.6283	14.743	1.417		–41.55	31
3470	190.1033	–60.7195	13.922	1.599		–40.70	47
ID and photometric data were taken from Carraro et al. (2010)							
NGC 4815							
1795	194.3518	–64.9215	13.482		2.273	–30.11	65
358	194.4303	–64.9607	13.703		1.946	–31.12	63
210	194.4796	–64.9801	14.043		1.841	–29.92	53
95	194.4804	–64.9482	14.128		1.730	–30.75	49
106	194.5109	–64.9470	14.158		1.896	–30.60	46
Photometric data from Prisinzano et al. (2001)							
NGC 6705							
2000	282.6180	–6.2534	11.428	1.587		34.42	81
1837	282.6552	–6.2434	12.001	1.422		35.28	131
1658	282.6901	–6.2011	11.622	1.475		35.13	111
1625	282.6974	–6.2884	11.652	1.729		32.01	102
1446	282.7289	–6.2717	11.860	1.468		34.76	104
1423	282.7325	–6.3041	11.414	1.627		35.23	121

Table 1.1 – continued from previous page

ID	l	b	V	$B-V$	$V-I$	RV	S/N
	deg (J2000)	deg (J2000)	mag	mag	mag	km s^{-1}	
1364	282.7398	–6.2295	11.830	1.211		30.60	162
1286	282.7477	–6.2121	11.872	1.398		34.38	117
1256	282.7510	–6.2832	11.586	1.733		35.23	88
1248	282.7513	–6.2884	12.081	1.461		35.23	122
1184	282.7583	–6.2907	11.426	1.604		32.03	81
1145	282.7620	–6.2584	12.014	1.453		32.76	118
1117	282.7642	–6.2723	11.801	1.438		36.14	105
1111	282.7649	–6.2698	11.902	1.418		34.63	113
1090	282.7666	–6.3448	11.872	1.566		34.01	102
963	282.7776	–6.2123	11.720	1.510		33.23	113
916	282.7828	–6.2866	11.621	1.463		33.86	188
899	282.7847	–6.2814	11.736	1.466		33.14	94
827	282.7922	–6.2635	11.493	1.503		36.88	115
816	282.7937	–6.2631	11.627	1.507		33.08	121
779	282.7965	–6.2428	11.468	1.732		33.42	87
686	282.8105	–6.2820	11.923	1.480		35.15	97
669	282.8139	–6.3100	11.974	1.553		33.75	161
660	282.8155	–6.3041	11.807	1.490		35.17	139
411	282.8609	–6.2483	11.559	1.669		33.90	128
160	282.9181	–6.2869	11.525	1.539		33.25	121
136	282.9221	–6.3368	11.849	1.499		33.21	83
ID and photometric data were taken from Sung et al. (1999)							
Collinder 261							
RGB02	301.6504	–05.5531	12.94	1.45		−25.63	100-130
RGB05	301.7076	–05.5238	14.14	1.34		−27.09	70-100
RGB06	301.6998	–05.5353	14.01	1.37		−24.91	80-100
RGB07	301.6813	–05.5377	14.01	1.38		−25.70	60-100
RGB09	301.7060	–05.5018	14.21	1.34		−25.96	80-120
RGB10	301.6787	–05.5247	14.37	1.31		−25.32	60-90

Table 1.1 – continued from previous page

ID	l	b	V	$B-V$	$V-I$	RV	S/N
	deg (J2000)	deg (J2000)	mag	mag	mag	km s^{-1}	
RGB11	301.6894	–05.5579	14.15	1.29		−23.42	80-100
For ID and photometric data references see Sestito et al. (2008)							
Melotte 66							
1346	259.6148	–14.2862	14.59		1.23	21.55	80-110
1493	259.6168	–14.2336	14.68		1.29	21.32	80-100
1785	259.5489	–14.3024	14.59		1.24	21.60	90-110
1884	259.5596	–14.2534	14.71		1.19	21.04	80-100
2218	259.5314	–14.2199	14.48		1.19	20.72	100-115
For ID and photometric references see Sestito et al. (2008)							
NGC 4609							
43	301.9865	–00.0553	9.34	1.43		−20.74	∼180
ID and photometric values from Feinstein & Marraco (1971)							
NGC 5316							
31	310.1919	+00.1544	9.39	1.43		−13.50	∼200
35	310.1819	+00.1307	9.44	1.48		−15.03	∼200
45	310.2426	+00.1333	9.55	1.61		−13.79	∼200
72	310.2247	+00.1239	9.84	1.59		−15.52	∼150
Photometry values from Carraro & Seleznev (2012)							
NGC 2324							
850	213.3859	+03.3012	13.351		1.135	39.07	80-85
2603	213.5001	+03.2390	12.530		1.479	42.14	150-180
2225	213.4774	+03.2667	13.422		1.139	45.85	95-130
1006	213.4107	+03.3217	13.291		1.147	34.91	100-110
1992	213.4865	+03.3201	12.580		1.266	41.78	130-180
1788	213.4687	+03.3170	13.608		1.142	41.82	85-105
2027	213.4855	+03.3141	13.325		1.153	37.65	95.115
For ID and photometric references see Bragaglia et al. (2008)							

Table 1.1 – continued from previous page

ID	l	b	V	$B-V$	$V-I$	RV	S/N
	deg (J2000)	deg (J2000)	mag	mag	mag	km s^{-1}	
			NGC 2477				
13385	253.6876	-05.8522	12.771	1.237		7.02	95-130
4221	253.6955	–05.8145	12.231	1.197		8.27	115-150
5035	253.6148	–05.8647	12.306	1.217		6.71	135-190
3206	253.6582	–05.7229	12.321	1.223		6.80	130-190
2061	253.6220	–05.7516	12.710	1.204		8.06	100-135
8039	253.5049	–05.8386	12.320	1.226		8.18	125-165
		For ID and photometric references see Bragaglia et al. (2008)					
			NGC 3960				
310755	294.3762	+06.1470	13.512	1.285		−24.16	120-130
310756	294.3609	+06.1604	13.194	1.172		−22.39	95 -115
310757	294.3809	+06.1569	13.062	1.261		−21.94	110-130
310758	294.3531	+06.1780	12.945	1.139		−21.86	115-160
310760	294.3773	+06.1876	13.060	1.164		−32.87	120-190
310761	294.3763	+06.1961	13.100	1.209		−22.58	100-110
		For ID and photometric references see Sestito et al. (2006)					

1.3 Observations

The spectra analysed in this work were observed by co-authors using two spectrographs. NGC 4815, NGC 6705 ant Trumpler 20 were observed on the Very Large Telescope (VLT) in Chile using UVES spectrograph by colleagues from the Gaia-ESO consortium. Spectra of stars in NGC 4609 and NGC 5316 were observed by our colleague R. Smiljanic, who used FEROS spectrograph mounted at the 2.2 m MPG/ESO Telescope in La Silla, Chile. Spectra for stars in the open clusters NGC 2324, NGC 2477, NGC 3960, Collinder 261 and Melotte 66 were observed by colleagues from the BOCCE consortium using UVES spectrograph on the VLT tele-

scope in Chile. In total for the analysis there were spectra of 110 stars belonging to ten open clusters.

1.3.1 UVES spectrograph

105 spectra in our analysis were observed with the FLAMES (Fiber Large Array Multi-Element Spectrograph) multi-fiber facility (Pasquini et al. 2002). Spectra of high-resolving power (R = 48000) were obtained with UVES (Ultraviolet and Visual Échelle Spectrograph, Dekker et al. 2000). For the objects in the Gaia-ESO survey, the spectra were exposed onto two CCDs, resulting in a wavelength coverage of 4700-6840 Å with a gap of about 50 Å in the centre. The spectra were reduced with the ESO UVES pipeline and dedicated scripts described by Sacco et al. (2014).

For the BOCCE project the same spectrograph was used, however, the clusters were observed with both the RED580 (wavelength range ∼4750 - 6800 Å) and RED860 (wavelength range ∼6600 - 10600 Å) configurations. Details of observations and reductions are presented in the paper by Sestito et al. (2008). The signal-to-noise ratios of the analysed spectra are presented in Table 1.1.

1.3.2 FEROS spectrograph

The observations for the five stars in NGC 4609 and NGC 5316 were carried out using bench-mounted, high-resolution, environmentally controlled, astronomical Échelle spectrograph FEROS (Fiber-fed Extended Range Optical Spectrograph) at the 2.2m Max Planck Gesellschaft/European Southern Observatory (ESO) Telescope in La Silla, between 22-30 of June 2010. FEROS provides a full wavelength coverage of 3500 - 9200 Å over 39 orders with resolving power of 48000. All spectra were reduced with the FEROS DRS (Data Reduction System) pipeline within MIDAS. Details of observations and signal-to-noise ratios of the spectra are presented in Table 1.1.

Chapter 2

Method of analysis

2.1 Differential analysis

The analysis technique adopted in this work is called a classical differential analysis method. As the name suggests, we chose a well studied (so called standard) star, and we make our analysis in relation to that star - in our case it was the Sun. We adopted a dual approach in calculating the abundances of chemical elements: a method of equivalent widths and spectral synthesis. The method of equivalent widths was used for the chemical elements which have many unblended lines in the stellar spectra, while the spectral synthesis method was applied for chemical elements which can be investigated using molecular bands or from a single weak line, for example oxygen.

2.2 Equivalent width method

The information on stellar atmosphere parameters is hidden in the spectral lines of a star. By analysing the selected spectral features, we can gain information on the surface temperature of the star, free fall acceleration rate at the surface, the rotation speed of the star etc. The equivalent width is the main parameter of a spectral line and it is described as total absorption of radiation as indicated by a spectral feature. It is found by forming a rectangle with a height of the normalized continuum emission, and finding a width such that the area of the rectangle is equal to the area of the spectral line. It is described as a following equation:

$$W_\lambda = \sum \frac{F_c - F_\lambda}{F_c} d\lambda \tag{2.1}$$

Where W_λ is the equivalent width, $F_c = 1$ is the intensity of a continuum, F_λ

- intensity at a given wavelength and $d\lambda$ is the wavelength interval. The W_λ is measured as length in Å.

In this work we used two software packages to measure equivalent widths. The first one is the automated DAOSPEC package, maintained by Peter B. Stetson from Dominion Astrophysical Observatory (Stetson & Pancino 2008), and the other one is SPLAT-VO, developed by German Astrophysical Virtual Observatory and the Astronomical Institute of the Academy of Sciences of the Czech Republic (Škoda et al. 2014). Both approaches required a careful consideration of spectral lines, as they had to be without visible contaminations or blending so we could get the most reliable results.

The automated DAOSPEC package was used to analyse the three open clusters from Gaia-ESO project (NGC 4815, NGC 6705, Trumpler 20) simply due to the sheer amount of objects that needed to be processed in short amount of time. The analysis involved other scientific groups, as Gaia-ESO is a joint project. More detailed description of the process for the Gaia-ESO objects will be presented in section 2.5.

SPLAT-VO was used for measurements of the lines in clusters NGC 4609 and NGC 5316. This software is more open, as we can inspect each fit visually and evaluate how good is the fit, and if any adjustments are necessary to the placement of the continuum or the fit itself.

We used equivalent widths of Fe I and Fe II lines for the determination of main atmospheric parameters ($T_{\rm eff}$, log g, metallicity and microturbulence velocity) and abundances of Na, Mg, Al, Si, Ca, Sc, Ti, V, Cr, Mn, Co, and Ni chemical elements. We have used from two lines (aluminium) to 18 lines (nickel) for abundance determinations. Each line for Na, Mg, Al, Si, Ca, Sc, Ti, V, Cr, Mn, Co, and Ni was inspected and some of them were excluded due to blending or other contamination effects, hence the line list differs slightly for every star. For this task we used the SPLAT-VO tool. For abundance calculations of the mentioned elements we used neutral lines, however, we determined the Ti II abundance from ionized lines as well.

The sodium abundance was determined from three or four lines (4751.8, 5682.6, 6154.2 and 6160.8 Å). We applied non-local thermodynamic equilibrium (NLTE) corrections as described in the paper by Lind et al. (2011). The magnesium abun-

dance was determined from equivalent widths of two or three Mg I lines (5711.09, 6318.70, and 6319.24 Å). Number of lines used for the determination of abundances of other elements are presented in Table 3.6.

As mentioned before, we used a differential analysis method which takes advantage of one (or more) standard stars with a well studied chemical composition. In our case it was the Sun. For all the lines that we used to calculate the elemental abundances, we first calculated the result using the Suns equivalent widths for the same lines. And the abundance that we determined was used for the differential analysis using the customary spectroscopic notation:

$$[\mathrm{X/Y}] \equiv \log_{10}(\mathrm{N_X/N_Y})_{\mathrm{star}} - \log_{10}(\mathrm{N_X/N_Y})_{\odot}. \tag{2.2}$$

Where N is the number of element atoms per unit of volume.

2.3 Spectral synthesis

2.3.1 Carbon, nitrogen and oxygen

In addition to equivalent widths method, we have adopted the spectral synthesis as well. For this task we used the BSYN software package, developed at the Uppsala University. This method takes main stellar parameters and spectral line data which we prepared using the Vienna atomic line database (VALD) (Kupka et al. 2000) and the paper by Gurtovenko & Kostyk (1989). From Gurtovenko & Kostyk (1989) we took the oscillator strengths for the measured lines. This method enables us to synthesise the spectra with the given parameters, and compare it to the observed one. By doing so, we can change the elemental abundances for selected lines in synthetic spectra, and by finding the best fit we can determine the abundances of various elements. This method is a differential method as well. To gain accurate results, synthetic spectrum had to be calibrated first. The calibration was done with the Kurucz (2005) solar spectra and the solar elemental abundances from Grevesse et al. (2007). The theoretical atomic oscillator strengths taken that were from VALD database were slightly changed to match the solar spectrum. This method requires the use of stellar atmosphere models - MARCS (see section 2.4).

This method was used to determine carbon, nitrogen abundances in all our target

stars (and oxygen when the lines were available). We used two regions for carbon abundance determination: C_2 Swan (0,1) band heads at 5135.5 Å and 5635.2 Å. The same molecular data of C_2 are used as by Gonzalez et al. (1998). For oxygen we used the forbidden [O I] line at 6300 Å. Lines of [O I] are considered as very good indicators of oxygen abundances as it was determined that they are not only insensitive to NLTE effects, but also give similar oxygen abundance results with 3D and 1D model atmospheres (c.f. Asplund 2004; Pereira et al. 2009). The gf values for ^{58}Ni and ^{60}Ni isotopic line components, which blend the oxygen line, were taken from Johansson et al. (2003). The nitrogen abundance was determined from different regions, depending on the available spectral wavelength coverage. For Gaia-ESO project clusters (NGC 4815, NGC 6705, Trumpler 20) the nitrogen abundance was determined from the interval 6470 – 6490 Å containing ^{12}C^{14}N bands, and for the other clusters we used an interval of 7980-8010 Å containing strong CN features. The CN molecular data for this wavelength interval were provided by Bertrand Plez. The example of spectral synthesis for carbon, nitrogen and oxygen are presented in Figs. 2.1 – 2.11.

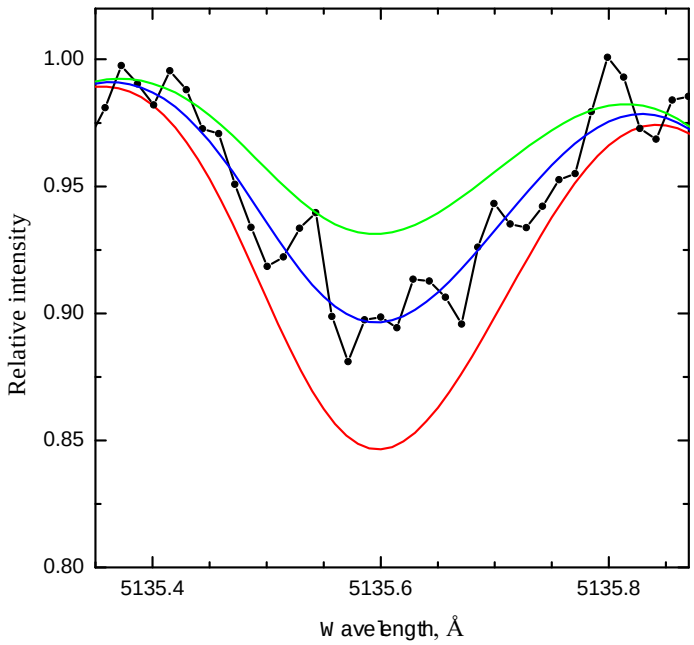

Figure 2.1: A fit to the C_2 Swan (1,0) band head at 5135 Å in the programme star Tr 20 63. The observed spectrum is shown as a black line with dots. The synthetic spectra with $[C/Fe] = -0.22 \pm 0.1$ are shown as coloured lines.

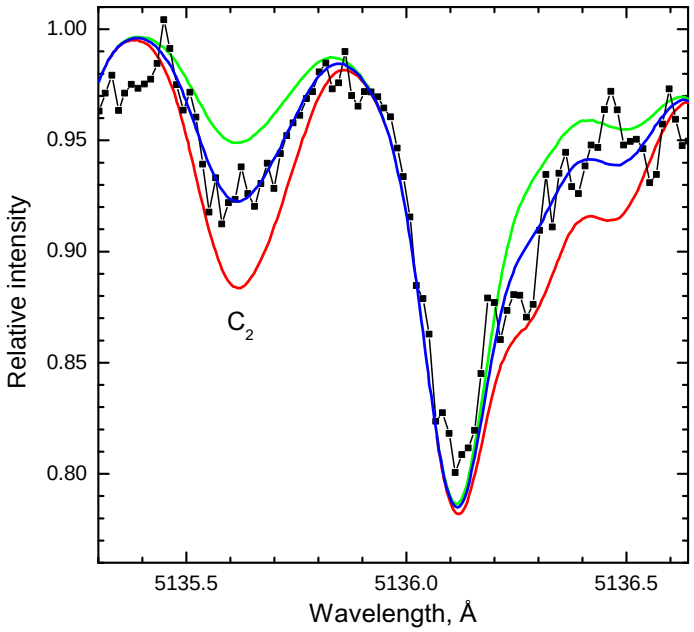

Figure 2.2: A fit to the C_2 Swan (1,0) band head at 5135 Å in the star NGC 2324 2027. The observed spectrum is shown as a black line with dots. The synthetic spectra with $[C/Fe] = -0.36 \pm 0.1$ are shown as coloured lines.

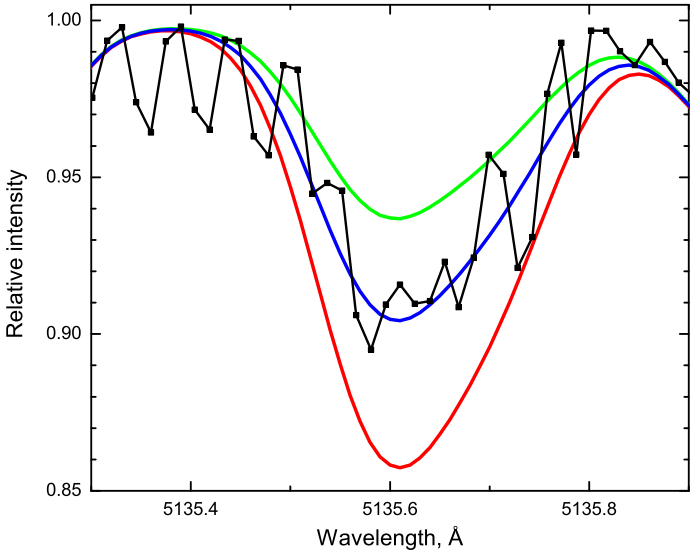

Figure 2.3: Fit to the C_2 Swan (1,0) band head at 5135 Å in the star Melotte 66 1785. The observed spectrum is shown as a black line with dots. The synthetic spectra with $[C/Fe] = -0.52$ is shown as a blue line and ± 0.1 dex as red and green lines.

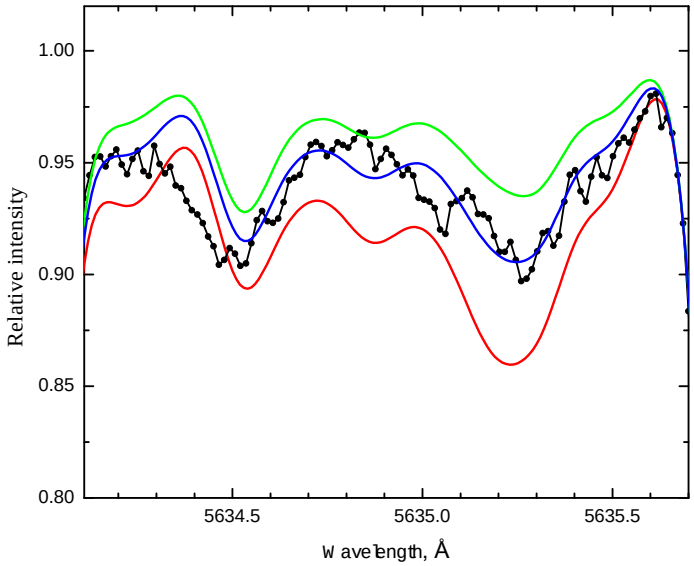

Figure 2.4: A fit to the C_2 Swan (0,1) band head at 5635.5 Å in the programme star NGC 4815 358. The observed spectrum is shown as a black line with dots. The synthetic spectra with $[C/Fe] = -0.16 \pm 0.1$ are shown as coloured lines.

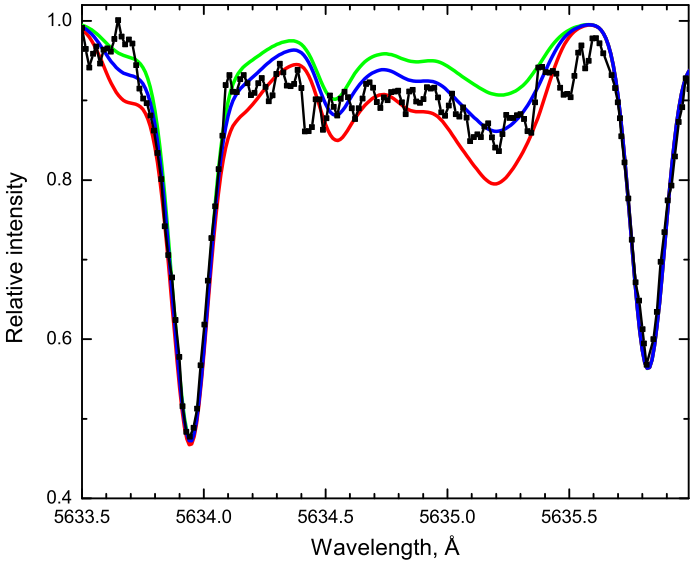

Figure 2.5: Fit to the C_2 Swan (0,1) band head at 5635.5 Å in the star Collinder 261 RGB05. The observed spectrum is shown as a black line with dots. The blue line is the synthetic spectra with $[C/Fe] = -0.1$ and the green and red lines show the abundance of ± 0.1 dex.

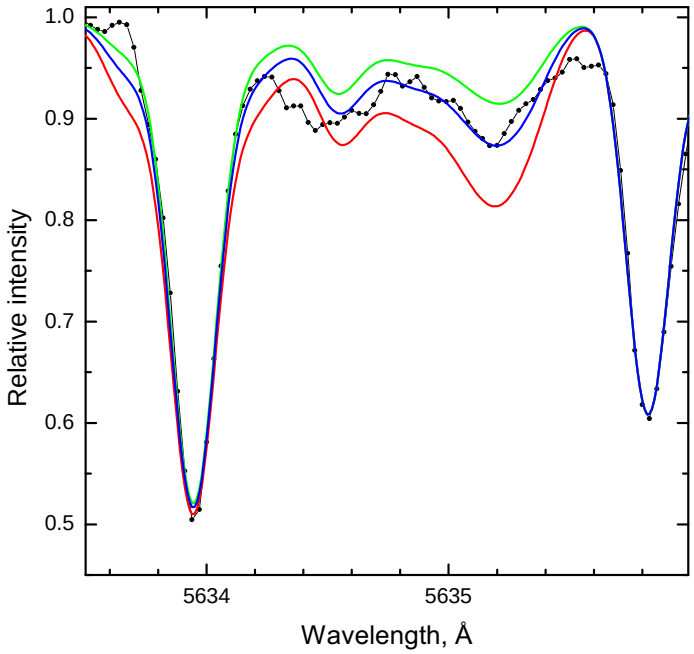

Figure 2.6: A fit to the C_2 Swan (0,1) band head at 5635.5 Å in the star NGC 5316 45.The observed spectrum is shown as a black line with dots. The synthetic spectra with $[C/Fe] = -0.08 \pm 0.1$ are shown as straight lines.

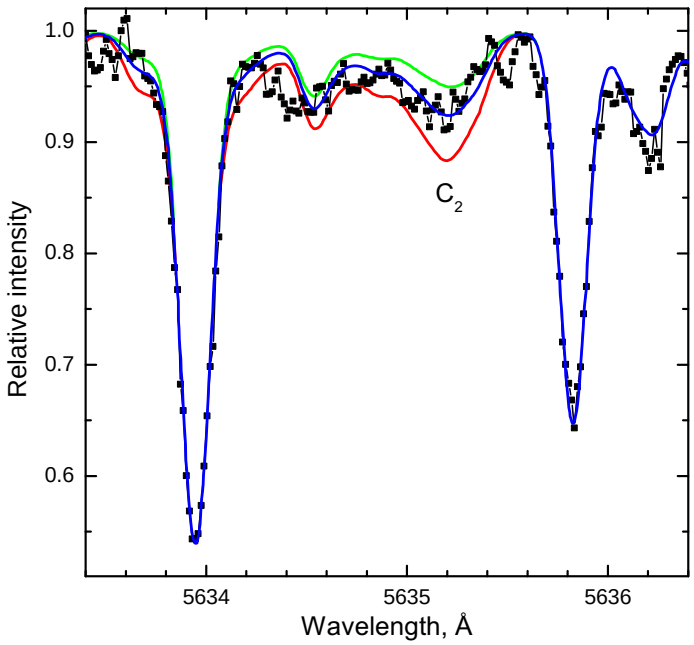

Figure 2.7: A fit to the C_2 Swan (0,1) band head at 5635.5 Å in the star NGC 2477 4221. The observed spectrum is shown as a black line with dots. The synthetic spectra with $[C/Fe] = -0.26 \pm 0.1$ are shown as coloured lines.

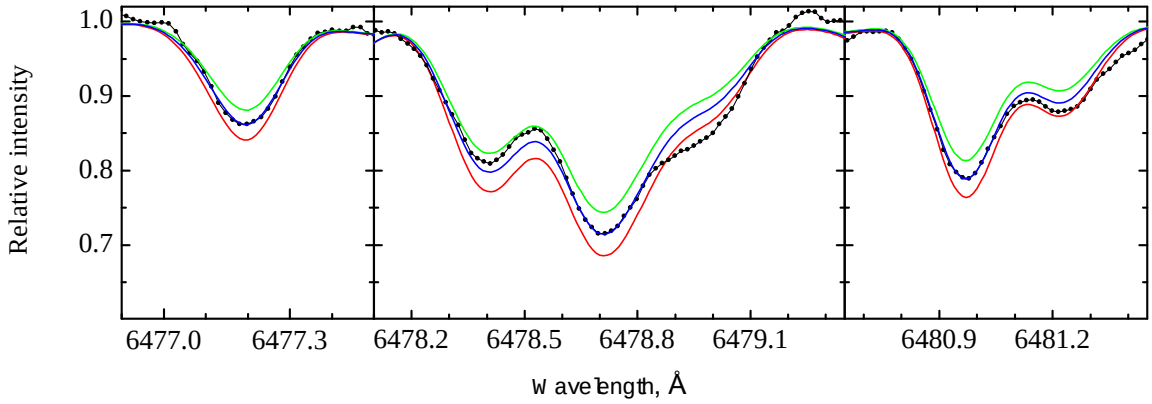

Figure 2.8: A fit to the CN bands in the programme star NGC 6705 1625. The observed spectrum is shown as a black line with dots. The synthetic spectra with $[\mathrm{N/Fe}] = 0.66 \pm 0.1$ are shown as coloured lines.

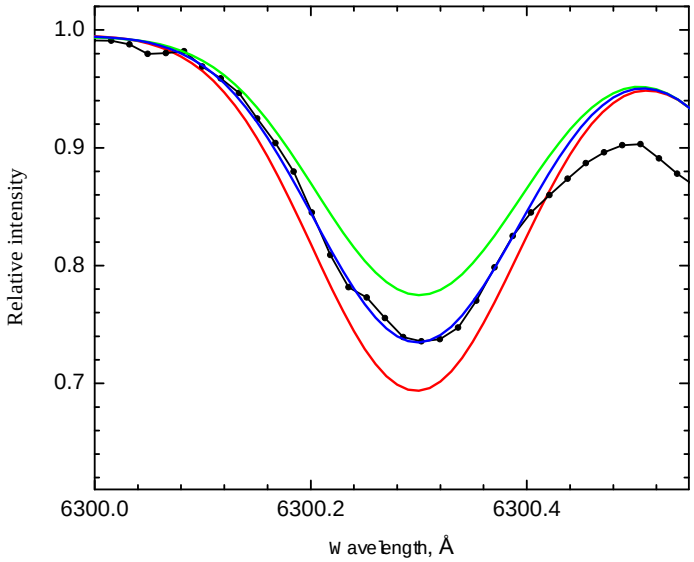

Figure 2.9: A fit to the forbidden [O I] line at 6300.3 Å in the programme star NGC 6705 779. The observed spectrum is shown as a black line with dots. The synthetic spectra with $[\mathrm{O/Fe}] = 0.07 \pm 0.1$ are shown as coloured lines.

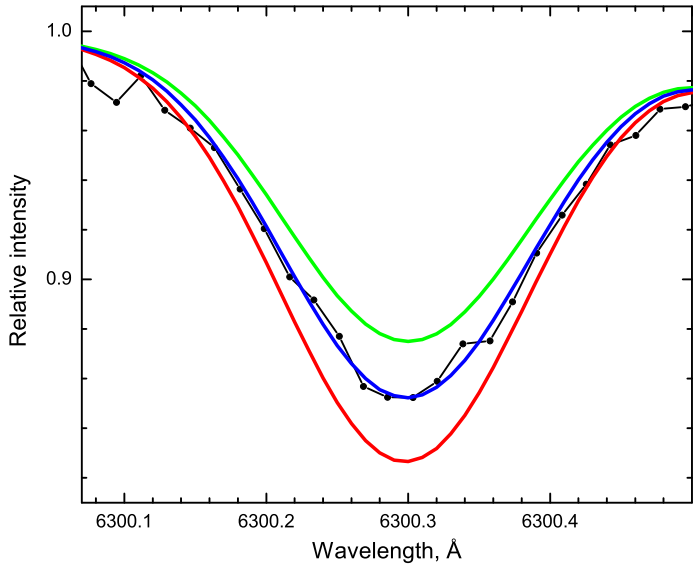

Figure 2.10: Fit to the forbidden [O I] line at 6300.3 Å in the spectrum of the star Melotte 66 1493. The observed spectrum is shown as a black line with dots. The synthetic spectra with $[O/Fe] = 0.2$ is shown as a blue line and ± 0.1 dex is shown as green and red lines.

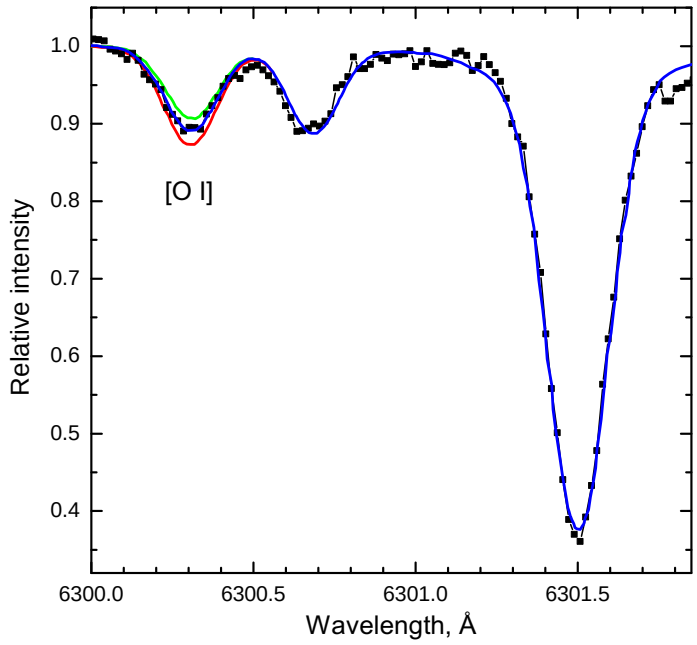

Figure 2.11: A fit to the forbidden [O I] line at 6300.3 Å in the spectrum of the star NGC 2477 4221. The observed spectrum is shown as a black line with dots. The synthetic spectra with $[O/Fe] = -0.08 \pm 0.1$ are shown as coloured lines.

2.3.2 $^{12}C/^{13}C$ ratio

The $^{12}C/^{13}C$ ratio was obtained from the $^{13}C/^{12}N$ feature at 8004.7 Å. This feature was analysed in seven open clusters: Collinder 261, Melotte 66, NGC 2324, NGC 2477, NGC 3960, NGC 4609 and NGC 5316. Unfortunately the spectra for stars of other clusters did not have the required wavelength coverage to analyse the $^{12}C/^{13}C$ ratios. The examples of the fits to the $^{12}C/^{13}C$ feature are displayed in Figs. 2.12 – 2.14.

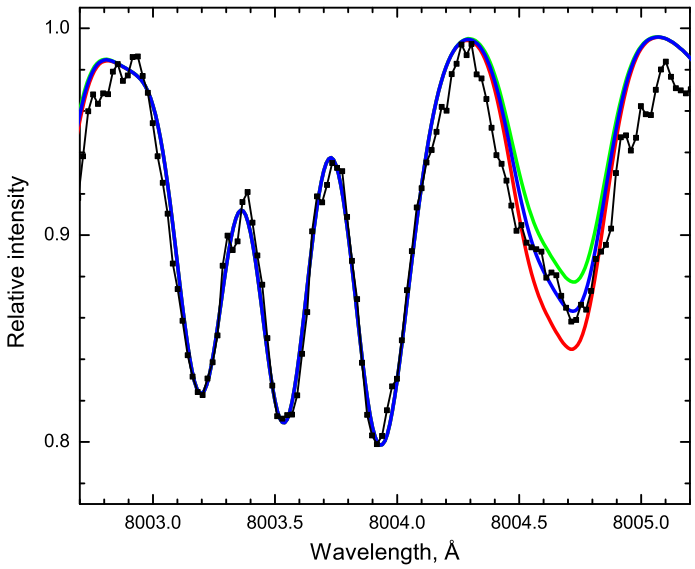

Figure 2.12: Fit to the CN bands in the star Melotte 66 1865. The observed spectrum is shown as a black line with dots. The synthetic spectra with $[\mathrm{N/Fe}] = 0.42$ and $^{12}C/^{13}C = 6$ is shown as a blue line and green and red lines represent ± 1 to the $^{12}C/^{13}C$ ratio.

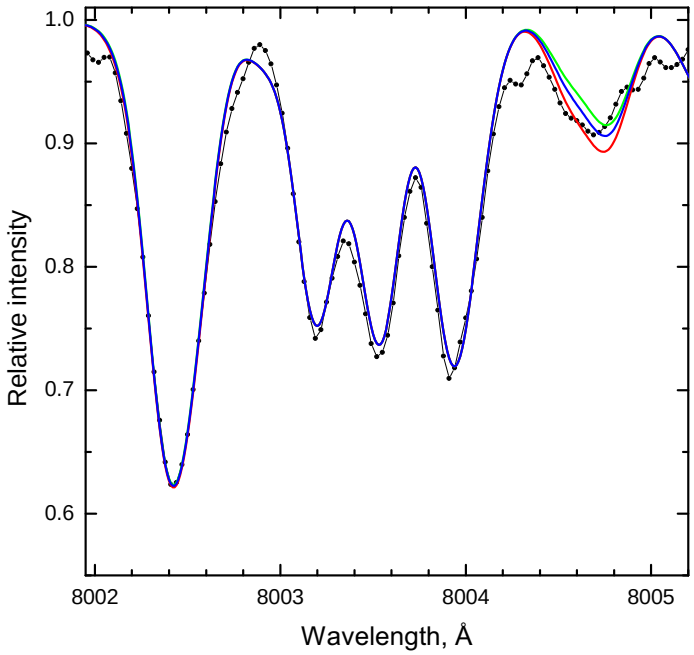

Figure 2.13: A fit to the CN bands in the star NGC 4609 43. The observed spectrum is shown as a black line with dots. The synthetic spectra with $^{12}C/^{13}C$ ratio 23 ± 5 are shown as straight lines

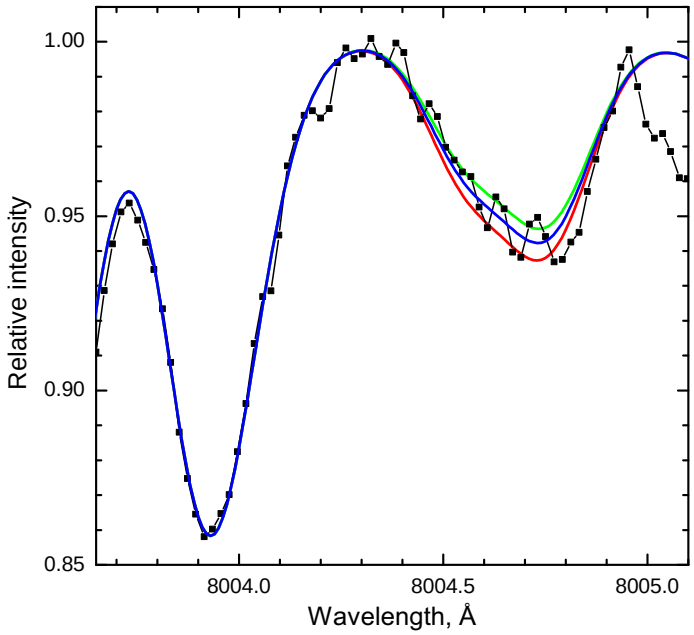

Figure 2.14: A fit to the CN bands at 8002–8006 Å in the star NGC 3960 310757. The blue line represents [N/Fe]=0.31 and $^{12}C/^{13}C$=10, with other two lines showing $+1$ (green line) and -1 (red line) to the $^{12}C/^{13}C$ ratio.

2.4 Model atmospheres

The formation of absorption lines in stellar spectra are influenced by many different processes that take place in the atmospheres of stars. We can analyse and interpret the data by using model atmospheres, in this case - MARCS models (Gustafsson et al. 2008). These models provide the theoretical data of how the different parameters of stellar atmosphere at different depths impact the formation of spectral lines. Hydrostatic equilibrium, energy transfer equations and other thermodynamic statistics and quantum mechanics equations are taken into account when calculating these models.

As already mentioned, we used a set of plane-parallel one-dimensional hydrostatic LTE (local thermal equilibrium) model atmospheres with constant flux taken from the MARCS stellar model atmosphere and flux library[1] was described by Gustafsson et al. (2008). The MARCS database contains over 50 000 stellar models for F-, G-, K-spectral class stars, spanning different temperature ranges, gravities and metallicities. The $T_{\rm eff}$ is covered in the range of 2500 - 8000 K, the gravities (log g) range from -1.0 to 5.5, and the metallicities, [Fe/H], have a range from -5.0 to $+1.0$ dex. There is also the option to choose different microturbulence velocities. Models contain 56 layers of information in which atmospheric parameters are described. However they are calculated making a few assumptions:

- Stellar atmospheres are very thin compared to the radius of the star. The layers of the atmosphere are plane parallel and the physical variables depend on only one spherical coordinate.
- Stars are in hydrostatic equilibrium, the gravity is in balance with the pressure and depends on the optical depth.
- The photosphere is static - there is no significant mass movement inside the photosphere of any kind (there is no mass loss, no magnetic fields or pulsations).
- Local thermodynamic equilibrium (LTE) is accepted. Gas depends only on local radiation field, which does not interact with other layers of the atmosphere. Each layer has its own temperature.

[1] http://marcs.astro.uu.se/

Models for bright stars with low lg g (up to 3.5) are calculated using spherical symmetry approach and taking into account the different masses of stars. For stars with lg$g > 3.5$ plane parallel models were used. The solar elemental abundances used in MARCS calculations are those from Grevesse et al. (2007).

2.5 Main atmospheric parameter determination

Atmospheric parameters of stars were determined using the standard spectroscopic method. The effective temperature ($T_{\rm eff}$) was determined requiring that the abundance of Fe I lines did not depend on the lower level excitation potential (χ) of the lines. The surface gravities (log g) were determined from the iron ionization equilibrium. The microturbulence velocity ($v_{\rm t}$) was found by minimising a scatter between abundances of Fe I lines and assuming that there should be no relation between abundances and equivalent widths. Determining these three main parameters through multiple iterations provided us with the value of metallicity as calculated from the used Fe I lines.

For the open clusters NGC 4609 and NGC 5316 we used the SPLAT-VO program to measure the equivalent widths. The process is manual, with the possibility to inspect each line individually, which provides better accuracy for the results. For the parameter determination from the measured spectral line widths we used the Eqwidth package. This package makes the calculations and gives an abundance for a given model atmosphere. By changing the parameters of model atmospheres we can meet the criteria for $T_{\rm eff}$, lg g and microturbulence velocity.

The main atmospheric parameters of the stars included in the Gaia-ESO survey (NGC 4815, NGC 6705, Trumpler 20) were determined spectroscopically as well, using a technique described by Smiljanic et al. (2014). To make full use of the available expertise of the consortium, all the spectra were analysed in parallel by 13 nodes of scientists. The methodology and codes used by each Node are described in detail by Smiljanic et al. (2014). A number of constraints have been imposed on input data used in the analysis to guarantee a high degree of homogeneity in the final results: the use of a common line list, the use of one single set of model atmospheres, and the analysis of common calibration targets. The Gaia-ESO Survey line list version 4.0 was used to determine the main atmospheric parameters of the

cluster stars. For model atmospheres, the MARCS grid (Gustafsson et al. 2008) was adopted.

To homogenise the results of different nodes and quantify the method-to-method dispersion of each parameter the median and the associated median absolute deviation (MAD) have been used. The first step was a zeroth-order quality control of the results of each node (values with very large error bars were removed). Then, we used results of the benchmark stars to weight the performance of each node in different regions of the parameter space. Finally, the weighted-median value of the validated results was adopted as the recommended value of that parameter. For the Gaia-ESO survey Internal Data Release 2 results, used in this work, the median of the method-to-method dispersion is 55 K, 0.13 dex, and 0.07 dex for $T_{\rm eff}$, log g, and [Fe/H], respectively.

2.6 Uncertainties

Uncertainties can be divided into two categories. Firstly, there are errors that affect each line individually. Fitting of individual lines depends on several factors, including uncertainties on atomic parameters, continuum placement variations, and the fitting of synthetic spectra to each line. Secondly, there are errors that affect all measured lines simultaneously, such as uncertainties in the stellar atmospheric parameters used. To evaluate possible deviations of abundances related to the uncertainties of atmospheric parameters we assumed the typical error estimates of the atmospheric parameters which are $T_{\rm eff} \pm 100$ K, log $g \pm 0.3$ dex, $v_{\rm t} \pm 0.3$ km s^{-1} and $[{\rm Fe/H}] \pm 0.1$ dex. The sensitivity of the abundance estimates Δ[El/H] to changes in the atmospheric parameters are listed in Tables 2.1 – 2.4. Possible parameter errors do not affect the abundances seriously (in this case the deviations were calculated on the elemental abundance relative to hydrogen - [El/H]). Note that the effects on the abundances relative to iron [El/Fe] are often considerably lower.

Random errors of abundance determinations (mainly caused by uncertainties of the continuum placement and the oscillator strengths of individual lines as well as S/N ratios) can be evaluated from the scatter of abundances determined from different lines. For example the mean value of [C/H] scatter from the C_2 5135 and 5635.5 Å lines in Trumpler 20 is equal to $\pm$0.03 dex, in NGC 4815 $\pm$0.06 dex, and

in NGC 6705 ±0.02 dex. The same low mean values of scatter are found in the case of [N/H] as well. Since oxygen abundances were determined just from one line at 6300.3 Å, our ad hoc evaluation of random errors for [O/H] is ±0.05 dex in NGC 6705, and slightly larger, of about ±0.15 dex, in NGC 4815.

The influence of stellar rotation on the C, N, and O abundances in slowly rotating stars of our sample is very small; it becomes more important in stars rotating more rapidly. If $v \sin i$ is about 3 km s^{-1}, a difference of ±1 km s^{-1} changes the abundances only by ±0.01 dex. If $v \sin i$ is about 7 km s^{-1}, a difference of ±1 km s^{-1} changes the abundances of nitrogen and oxygen by about ±0.06 dex, while carbon abundances change only by ±0.02 dex.

Since abundances of C, N, and O are also bound together by molecular equilibrium in the stellar atmospheres, we investigated further how an error in one of them typically affects the abundance determination of another. Results are displayed are displayed in Table 2.5.

Table 2.1: Effects on derived abundances, Δ[El/H], resulting from model changes for the star NGC 6705 1625.

Species	$\Delta T_{\rm eff}$ ±100 K	$\Delta \log g$ ±0.3	$\Delta v_{\rm t}$ ±0.3 km s^{-1}	Δ[Fe/H] ±0.1	Total
C (C_2)	0.03	0.05	0.00	0.05	0.07
N (CN)	0.07	0.13	0.01	0.11	0.18
O ([O I])	0.01	0.12	0.00	0.01	0.12

Table 2.3: Effects on derived abundances, Δ[A/H], resulting from model changes for the star NGC 4609 43.

Species	$\Delta T_{\rm eff}$ ± 100 K	$\Delta \log g$ ± 0.3	$\Delta v_{\rm t}$ ± 0.3 km s^{-1}	Δ[Fe/H] ± 0.1	Total
C_2	0.01	0.08	0.00	0.02	0.08
CN	0.05	0.07	0.01	0.02	0.09
O I	0.01	0.13	0.00	0.03	0.13
$^{12}C/^{13}C$	1	1	0	0	1.4
Na I LTE	0.09	0.04	0.10	0.03	0.14
Mg I	0.02	0.02	0.04	0.01	0.05
Al I	0.08	0.01	0.07	0.02	0.11
Si I	0.05	0.07	0.08	0.01	0.12
Ca I	0.11	0.01	0.13	0.02	0.17
Sc I	0.02	0.13	0.11	0.04	0.18
Ti I	0.14	0.01	0.13	0.02	0.19
Ti II	0.02	0.13	0.13	0.04	0.19
Cr I	0.10	0.01	0.15	0.02	0.18
Mn I	0.09	0.06	0.16	0.03	0.20
Co I	0.04	0.06	0.15	0.02	0.17
Ni I	0.01	0.06	0.16	0.11	0.20

Table 2.2: Effects on derived abundances, Δ[A/H], resulting from model changes for the star Melotte 66 1493.

Species	$\Delta T_{\rm eff}$ ± 100 K	$\Delta \log g$ ± 0.3	$\Delta v_{\rm t}$ ± 0.3 km s^{-1}	Δ[Fe/H] ± 0.1	Total
C	0.01	0.08	0.00	0.02	0.08
N	0.05	0.07	0.01	0.02	0.09
O	0.01	0.13	0.00	0.03	0.13
$^{12}C/^{13}C$	1	1	0	0	1.4

Table 2.4: Effects on derived abundances, Δ[A/H], resulting from model changes for the star NGC 3960 310757.

Species	$\Delta T_{\rm eff}$ ± 100 K	$\Delta \log g$ ± 0.3	$\Delta v_{\rm t}$ ± 0.3 km s^{-1}	Δ[Fe/H] ± 0.1	Total
C	0.01	0.03	0.00	0.04	0.03
N	0.06	0.07	0.01	0.10	0.08
O	0.01	0.15	0.00	0.04	0.09
C/N	0.11	0.03	0.02	0.12	0.10
^{12}C/^{13}C	2	2	0	3	2

Table 2.5: Effects on derived abundances and isotopic ratios for the sample of target stars, resulting from abundance changes of C, N, or O.

Species	Δ C ± 0.1 dex	Δ N ± 0.1 dex	Δ O ± 0.1 dex
NGC 6705 1625			
Δ C	–	0.00	0.05
Δ N	0.17	–	0.12
Δ O	0.02	0.00	–
Melotte 66 1493			
Δ C	–	0.00	0.04
Δ N	0.10	–	0.08
Δ O	0.02	0.00	–
NGC 3960 310757			
Δ C	–	0.01	0.03
Δ N	0.12	–	0.06
Δ O	0.01	0.01	–
Δ C/N	0.19	0.16	0.02
Δ^{12}C/^{13}C	3	3	0

Chapter 3

Results and discussion

3.1 Main atmospheric parameters

In this section we present the main atmospheric parameters adopted for analysis of the target stars. Effective temperature, gravity, metallicity and microturbulence velocities for NGC 4815, NGC 6705 and Trumpler 20 were determined in the frame of the Gaia-ESO project, using the previously described method to homogenize the parameters determined by Vilnius and other groups of the network. Parameters for the clusters Collinder 261 and Melotte 66 were taken from Sestito et al. (2008). For NGC 2324 and NGC 2477 we adopted parameters derived by Bragaglia et al. (2008). Sestito et al. (2006) determined the parameters for NGC 3960. We used the spectroscopic approach and determined the parameters for clusters NGC 4609 and NGC 5316 as they had no previous parameter determinations. All adopted stellar parameters are presented in Table 3.1. Although taken from different sources, all parameters were determined spectroscopically albeit with only slight methodology deviations.

Table 3.1: Atmospheric parameters of stars in target clusters

ID	$T_{\rm eff}$ (K)	log g	v_t (km s^{-1})	[Fe/H]
Collinder 261				
Parameters adopted from Sestito et al. (2008)				
RGB02	4350	1.70	1.25	0.12
RGB05	4600	2.00	1.24	0.14
RGB06	4500	2.30	1.18	0.16
RGB07	4546	2.15	1.20	0.18
RGB09	4720	2.05	1.27	0.04

Table 3.1 – continued from previous page

ID	$T_{\rm eff}$ (K)	log g	v_t (km s^{-1})	[Fe/H]
RGB10	4700	2.35	1.20	0.20
RGB11	4670	2.15	1.13	0.09
Melotte 66				
Parameters adopted from Sestito et al. (2008)				
1346	4750	2.00	1.17	−0.37
1493	4770	2.15	1.20	−0.35
1785	4770	2.05	1.20	−0.30
1884	4750	2.45	1.23	−0.30
2218	4850	2.39	1.25	−0.31
NGC 2324				
Parameters adopted from Sestito et al. (2006)				
850	5100	2.20	1.21	−0.17
2603	4300	1.00	1.37	−0.14
2225	5060	2.10	1.23	−0.17
1006	5040	2.25	1.21	−0.17
1992	4750	1.65	1.29	−0.10
1788	5000	2.10	1.22	−0.27
2027	5000	1.84	1.26	−0.17
NGC 2477				
Parameters adopted from Sestito et al. (2006)				
13385	4980	2.80	1.14	0.05
4221	4970	2.68	1.15	0.05
5035	5000	2.70	1.15	0.10
3206	4950	2.66	1.16	0.05
2061	5030	2.67	1.15	0.07
8039	4970	2.65	1.16	0.12
NGC 3960				
Parameters adopted from Bragaglia et al. (2008)				
310755	4950	2.35	1.19	0.00
310756	5050	2.54	1.17	0.07

Table 3.1 – continued from previous page

ID	$T_{\rm eff}$ (K)	log g	v_t (km s^{-1})	[Fe/H]
310757	4870	2.16	1.22	0.00
310758	4950	2.4	1.19	0.02
310760	5040	2.57	1.18	0.00
310761	5000	2.45	1.18	0.02
NGC 4609				
Parameters determined in this work				
43	4620	2.20	1.45	0.16
NGC 4815				
Parameters determined in this work				
1795	4328	1.88	1.67	0.01
358	4905	2.56	1.89	−0.07
210	4964	2.76	1.59	0.02
95	5062	2.68	1.13	−0.04
106	4966	2.52	1.72	0.01
NGC 5316				
Parameters determined in this work				
31	4825	1.70	1.85	0.05
35	4650	2.00	2.05	−0.03
45	4500	1.80	1.85	−0.05
72	4450	1.80	1.75	−0.04
NGC 6705				
Parameters determined in this work				
2000	4543	1.82	1.83	−0.05
1837	4889	2.73	1.68	0.07
1658	4635	2.14	1.62	−0.07
1625	4330	1.71	1.64	−0.01
1446	4639	2.24	1.55	−0.05
1423	4496	1.94	1.73	0.07
1364	4828	2.55	1.40	0.02
1286	4883	2.43	1.61	0.01

Table 3.1 – continued from previous page

ID	$T_{\rm eff}$ (K)	log g	v_t (km s^{-1})	[Fe/H]
1256	4351	1.85	1.75	−0.04
1248	4867	2.39	1.73	0.07
1184	4321	1.80	1.60	−0.01
1145	4751	2.35	1.52	0.00
1117	4798	2.16	1.89	0.06
1111	4810	2.31	1.77	0.02
1090	4660	2.09	1.71	−0.03
963	4698	2.07	1.80	−0.02
916	4767	2.48	1.87	0.06
899	4713	2.19	1.83	0.05
827	4540	2.09	1.54	−0.07
816	4688	2.06	1.81	−0.14
779	4332	1.74	1.67	0.01
686	4730	2.25	1.86	−0.04
669	4675	2.18	1.85	0.08
660	4706	2.11	1.73	0.06
411	4422	1.97	1.62	0.03
160	4653	2.02	1.75	0.01
136	4687	2.13	1.73	0.01
Trumpler 20				
Parameters determined in this work				
2730	5006	3.11	1.43	0.18
2690	4863	2.84	1.23	0.21
63	4488	2.13	1.48	0.00
292	4494	2.17	1.49	0.02
1082	5017	2.99	1.39	0.13
724	5007	3.07	1.20	0.08
794	4516	2.17	1.57	−0.04
582	5003	3.09	1.34	0.20
542	4990	3.12	1.35	0.20
340	4873	2.99	1.37	−0.03

Table 3.1 – continued from previous page

ID	$T_{\rm eff}$ (K)	log g	v_t (km s^{-1})	[Fe/H]
770	5086	3.24	1.39	0.14
950	4967	2.90	1.45	0.06
505	4830	2.70	1.46	0.06
894	5000	3.09	1.39	0.11
203	5030	3.10	1.38	0.14
835	4931	3.00	1.43	0.08
1010	4976	2.94	1.42	0.15
923	5033	3.09	1.40	0.14
858	4889	2.92	1.39	0.13
227	5029	3.05	1.49	0.14
346	4990	3.03	1.40	0.17
781	4895	2.86	1.43	0.09
768	4955	3.00	1.36	0.22
791	4936	2.95	1.42	0.06
287	4984	2.97	1.42	0.08
1008	4570	2.20	1.57	−0.05
795	4918	2.92	1.47	0.12
246	4919	2.78	1.49	0.05
787	4949	2.95	1.41	0.17
638	4923	2.93	1.34	0.11
430	5954	3.65	1.50	0.12
827	4918	2.91	1.36	0.13
885	4964	3.00	1.40	0.09
399	4898	2.89	1.42	0.12
129	4910	2.99	1.37	0.13
429	4879	2.94	1.40	0.14
911	4503	2.12	1.53	−0.03
1044	4993	3.13	1.33	0.19
591	4369	2.06	1.51	−0.05
468	4431	2.08	1.55	0.01
679	4969	2.95	1.46	0.09

Table 3.1 – continued from previous page

ID	$T_{\rm eff}$ (K)	log g	v_t (km s^{-1})	[Fe/H]
3470	4570	2.24	1.57	−0.04

3.2 Evolutionary mixing processes

When we look at the stellar spectrum, we mostly see the same chemical composition from the time when the star was born. However that is not true for all chemical elements - nuclear synthesis is what drives the stellar evolution, and different elements or their isotopes are produced or destroyed during this process. The star spends most of its lifetime on the main sequence (MS) of the Herzprung-Russell diagram, burning hydrogen (converting hydrogen to helium) in the core. Once the star leaves the main sequence, the properties of the stellar interior change, and this can invoke the consequent changes of material transportation inside the star. The standard stellar evolution theory predicts that once the star leaves the MS and enters RGB, there is a mixing event, the so called first dredge-up, that brings the core processed material to the surface (Iben 1967). At this phase, the convective envelope of the star deepens and reaches the previously undisturbed layer of hydrogen fusion products – mainly ^{3}He, ^{7}Li, ^{12}C, ^{13}C, ^{14}N etc. Among the most noticeable changes in stellar surface abundances caused by the first dredge-up are the alterations of ^{12}C, ^{13}C and ^{14}N which are reflected in the decrease of ^{12}C/^{13}C and ^{12}C/^{14}N ratios.

The abundances of carbon and nitrogen and ratio of their specific isotopes are key tools for understanding of stellar mixing processes. The alterations of the abundances and ratios of these elements are the main indicators of mixing in stellar interiors. A number of scientist have worked on this topic and there are already a number of publications (Smiljanic et al. 2009; Tautvaišienė et al. 2000, 2001, 2005; Tautvaišienė & Puzeras 2009; Tautvaišienė et al. 2010; Barisevičius et al. 2010, 2011; Gratton et al. 1999, 2006; Gilroy 1989; Gilroy & Brown 1991; Luck 1994; Gonzalez et al. 1998; Gonzalez & Wallerstein 2000; Origlia et al. 2006; Sneden & Pilachowski 1986 etc.). The main aim of this work is to further study these elements and their changes in evolved stars as there is still not enough data for statistical

treatment of observational results in the whole range of turn-off masses which are covered by theoretical modelling.

3.2.1 Abundances of carbon and nitrogen, ratios of $^{12}C/^{13}C$ and C/N

Collinder 261 We find that the average value of carbon to iron ratio in Collinder 261 is [C/Fe]=-0.23 ± 0.02. When compared with the carbon values in galactic disk field dwarf stars we can see, that carbon is depleted by about 0.3 dex. The nitrogen to iron ratio in this cluster is [N/Fe]=0.18 ± 0.09, which is about 0.2 dex higher than in the field stars. The mean $^{12}C/^{13}C$ ratio in this cluster is 11 ± 2 for clump giants. We note, that the one star with the higher $^{12}C/^{13}C$ ratio of 18 is a first ascent giant. The mean C/N ratio in the clump stars are 1.6 ± 0.3 and a higher value of 1.74 was obtained for the first-ascent giant. Same discrepancies between clump and first-ascent giant in this cluster stars were found by Mikolaitis et al. (2012) who reported almost exactly the same values but for different stars. Our results are presented in Table 3.2.

Melotte 66 The determined average [C/Fe] ratio for this cluster is -0.27 ± 0.07 dex which is about 0.4 dex lower than previously determined values for galactic disk dwarf stars. The mean nitrogen-to-iron abundance is 0.17 ± 0.07 which lie above the determined value for field stars by about 0.2 dex. All stars analysed for this cluster are in the red clump, and our determined value for the average $^{12}C/^{13}C$ ratio is 8 ± 2. The mean C/N ratio for the stars of this cluster is 1.67 ± 0.21 dex. Results are displayed in Table 3.2.

NGC 2234 Results we obtained for this cluster are presented in Table 3.3. We have determined carbon, nitrogen and consequently the C/N ratios for this cluster. The determined average carbon content relatively to iron is [C/Fe]=-0.35 ± 0.06 which is lowered by about 0.4 dex from the galactic disk field stars. The nitrogen abundance is [N/Fe]=0.28 ± 0.05 and is by 0.3 dex larger than value for solar type stars. The determined $^{12}C/^{13}C$ ratio is equal to 21 ± 1 from four red giant stars. The calculated C/N ratio from seven RGB stars is equal to 0.92 ± 0.12 which is lower

than that of a solar value of ~ 4.00.

NGC 2477 The derived carbon to iron ratio in this cluster is [C/Fe]=-0.26 ± 0.02. It is lowered by approximately 0.3 dex from the initial values of solar type stars. The nitrogen value is [N/Fe]=0.39 ± 0.04 from six stars on the red giant branch. We derived the $^{12}C/^{13}C$ ratio of 20 ± 1 from four stars and C/N ratio of 0.91 ± 0.09 from six stars at the red clump position (see Table 3.3).

NGC 3960 Table 3.3 contains the elemental abundances we determined for this cluster. We investigated six stars at the red clump position in this cluster. The determined mean carbon-to-iron ratio is -0.39 ± 0.04 and we can see that it is depleted by about 0.4 dex when compared to solar type stars. The derived nitrogen content is [N/Fe]=0.32 ± 0.05. The mean C/N ratio calculated for the six stars is 0.80 ± 0.13. We also analysed the $^{12}C/^{13}C$ ratios and found that the mean value from seven stars is 16 ± 4. Both values are lowered from the solar content and show evidences of mixing processes.

NGC 4609 This cluster has not been previously analysed by high-resolution spectroscopy. From the CMD diagram we can see that this cluster has only a single star at the red clump position (see Fig. 1.6). The [C/Fe] value for this star is -0.23 ± 0.01 dex, as determined from two C_2 molecular bands. This is 0.3 dex lower than the average value for solar type stars in the galactic disk. The mean nitrogen-to-iron abundance derived from six $^{12}C^{14}N$ molecular features near 8000 Å is [N/Fe]=0.63 ± 0.02 and it is significantly higher (by 0.6 dex) when compared to galactic field stars. We determined both the $^{12}C/^{13}C$ and C/N ratios for this star. We obtained the $^{12}C/^{13}C$ ratio of 23 and C/N of 0.55. The results are presented in Table 3.4.

NGC 4815 We measured from five giants in NGC 4815 [C/Fe]=-0.16 ± 0.05 and [N/Fe]=0.54 ± 0.05. We see that carbon is depleted in these evolved stars compared to dwarf stars in our galactic disk by about 0.2 dex, and the nitrogen is enhanced by about 0.5 dex. The carbon-to-nitrogen ratio calculated from the respective abundances gives the value of 0.79 ± 0.08. Table 3.5 contains the values relative to

hydrogen, rather than to iron.

NGC 5316 This cluster is one of two (the other one being NGC 4609) which had no previous spectroscopic measurements. This cluster has four identified stars that are at the red clump position. The determined average carbon to iron value is [C/Fe]=-0.16 ± 0.07. This is about 0.2 dex lower than the determined value for galactic disk stars. The mean nitrogen content in four cluster stars [N/Fe] is equal to 0.66 ± 0.12. It is larger than nitrogen content in disk stars by approximately 0.6 dex. In this work we have determined $^{12}C/^{13}C$ and C/N ratios which are 23 ± 1 and 0.64 ± 0.24, respectively. Results are displayed in Table 3.4.

NGC 6705 Table 3.6 shows the values we determined for NGC 6705. We obtain from 27 giants in this cluster the average values [C/Fe]=-0.08 ± 0.06 and [N/Fe]=0.61 ± 0.07. The calculated mean value of C/N ratio is 0.83 ± 0.19 which is affected by mixing processes and are significantly lower than the solar value.

Trumpler 20 The mean values of the elemental abundances in this cluster as determined from 42 stars are [C/Fe]=-0.20 ± 0.07 and [N/H]=0.40 ± 0.06 (see Table 3.7). The carbon-to-iron ratio is depleted by approximately 0.3 dex and nitrogen-to-iron is enhanced by 0.4 dex when compared to solar type dwarf stars. The determined C/N ratio is 0.98 ± 0.12 which is lower than the values for the stars before first dredge up. $^{12}C/^{13}C$ ratio could not be determined due to the lack of spectral coverage.

Table 3.2: The determined elemental abundances for stars in the open clusters Collinder 261 and Melotte 66

Star	[C/Fe]	σ	[N/Fe]	σ	[O/Fe]	σ	C/N	$^{12}C/^{13}C$	Evol.
				Collinder 261					
RGB02	−0.20	0.04	0.16	0.02	−0.10	0.05	1.74	18	g
RGB05	−0.27	0.04	−0.01	0.05	−0.09	0.05	2.19	8	c
RGB06	−0.21	0.05	0.29	0.04	0.09	0.05	1.26	13	c
RGB07	−0.23	0.01	0.20	0.02	0.01	0.05	1.48	–	c
RGB09	−0.21	0.07	0.25	0.02	−0.04	0.05	1.38	12	c
RGB10	−0.20	0.03	0.17	0.01	−0.05	0.05	1.70	–	c
RGB11	−0.23	0.01	0.17	0.03	−0.11	0.05	1.58	12	c
Average:	-0.23 ± 0.02		0.18 ± 0.09		-0.03 ± 0.07		1.60 ± 0.30	11 ± 2	
				Melotte 66					
1346	−0.32	0.02	0.13	0.03	0.13	0.05	1.41	8	c
1493	−0.19	0.01	0.12	0.04	0.20	0.05	1.95	8	c
1785	−0.23	0.01	0.10	0.05	0.10	0.05	1.86	6	c
1884	−0.10	0.01	0.28	0.03	0.22	0.05	1.66	–	c
2218	−0.21	0.01	0.23	0.07	0.14	0.05	1.45	10	c
Average:	-0.21 ± 0.07		0.17 ± 0.07		0.16 ± 0.04		1.67 ± 0.21	8 ± 2	

Table 3.3: Elemental abundances for stars in the open clusters NGC 2324, NGC 2477 and NGC 3960

Star	[C/Fe]	σ [C/Fe]	[N/Fe]	σ [N/Fe]	[O/Fe]	C/N	$^{12}C/^{13}C$
				NGC 2324			
850	−0.30	0.02	0.33	0.06	−0.22	0.93	–
2603*	−0.43	0.06	0.22	0.08	−0.28	0.89	22
2225	−0.35	0.01	0.27	0.03	−0.20	0.95	–
1006	−0.28	0.02	0.33	0.04	−0.05	0.98	20
1992*	−0.43	0.02	0.31	0.06	−0.12	0.72	20
1788	−0.33	0.06	0.22	0.02	−0.17	1.12	–
2027	−0.36	0.04	0.31	0.06	−0.36	0.85	20
Average	–0.35 ±0.06		0.28 ±0.05		–0.20 ±0.10	0.92 ±0.12	21 ± 1
				NGC 2477			
13385	−0.25	0.02	0.34	0.02	−0.14	1.02	18
4221	−0.26	0.01	0.39	0.01	−0.08	0.89	20
5035	−0.29	0.03	0.41	0.05	−0.17	0.79	–
3206	−0.25	0.04	0.44	0.06	0.00	0.81	20
2061	−0.26	0.01	0.34	0.06	−0.16	1.00	–
8039	−0.24	0.01	0.40	0.05	−0.09	0.91	20
Average	−0.26 ± 0.02		0.39 ± 0.04		−0.11 ± 0.06	0.91 ± 0.09	20 ± 1
				NGC 3960			
310755	−0.37	0.02	0.23	0.05	−0.13	1.00	–
310756	−0.40	0.02	0.37	0.03	−0.23	0.68	12
310757	−0.47	0.02	0.31	0.05	−0.25	0.66	10
310758	−0.37	0.03	0.31	0.03	−0.19	0.83	20
310760	−0.38	0.01	0.35	0.02	−0.25	0.74	16
310761	−0.34	0.04	0.32	0.04	−0.10	0.87	18
Average	−0.39 ± 0.04		0.32 ± 0.05		−0.19 ± 0.06	0.80 ± 0.13	16 ± 4

Table 3.4: Determined abundances and isotopic ratios in NGC 4609 and NGC 5316

Element	NGC 4609	NGC 5316	NGC 5316	NGC 5316	NGC 5316	NGC 5316
	43	31	35	45	72	Average
[C/Fe]	-0.23 ± 0.01 (2)	-0.26 ± 0.02 (2)	-0.10 ± 0.02 (2)	-0.08 ± 0.03 (2)	-0.20 ± 0.04 (2)	-0.16 ± 0.07
[N/Fe]	0.63 ± 0.02 (6)	0.60 ± 0.05 (6)	0.82 ± 0.07 (6)	0.50 ± 0.05 (6)	0.72 ± 0.08 (6)	0.66 ± 0.12
[O/Fe]	0.11 ± 0.05 (1)	-0.11 ± 0.05 (1)	0.20 ± 0.05 (1)	0.07 ± 0.05 (1)	0.05 ± 0.05 (1)	0.11 ± 0.11
C/N	0.55	0.54	0.48	1.05	0.48	0.64 ± 0.24
$^{12}C/^{13}C$	23	22	23	24	24	23 ± 1
$[Na/Fe]_{LTE}$	0.42 ± 0.08 (4)	0.39 ± 0.06 (3)	0.35 ± 0.03 (3)	0.33 ± 0.08 (3)	0.45 ± 0.03 (3)	0.38 ± 0.05
$[Na/Fe]_{NLTE}$	0.33 ± 0.05 (3)	0.27 ± 0.06 (3)	0.26 ± 0.05 (2)	0.22 ± 0.07 (3)	0.33 ± 0.05 (3)	0.27 ± 0.04
[Mg/Fe]	-0.06 ± 0.01 (2)	-0.09 ± 0.05 (3)	-0.05 ± 0.06 (3)	-0.01 ± 0.11 (2)	0.04 ± 0.09 (3)	-0.03 ± 0.05
[Al/Fe]	0.15 ± 0.01 (2)	0.11 ± 0.08 (2)	0.16 ± 0.05 (2)	0.12 ± 0.01 (2)	0.12 ± 0.05 (2)	0.13 ± 0.02
[Si/Fe]	0.13 ± 0.07 (10)	0.06 ± 0.03 (8)	0.12 ± 0.04 (7)	0.13 ± 0.05 (7)	0.20 ± 0.02 (7)	0.13 ± 0.05
[Ca/Fe]	0.07 ± 0.08 (7)	0.01 ± 0.04 (3)	0.11 ± 0.05 (6)	0.10 ± 0.08 (5)	0.13 ± 0.02 (5)	0.09 ± 0.05
[Sc/Fe]	0.01 ± 0.04 (5)	0.07 ± 0.09 (3)	-0.05 ± 0.02 (3)	-0.05 ± 0.01 (3)	0.06 ± 0.03 (4)	0.01 ± 0.06
[Ti I/Fe]	0.02 ± 0.07 (17)	0.02 ± 0.07 (12)	-0.02 ± 0.03 (10)	0.06 ± 0.02 (12)	0.07 ± 0.06 (13)	0.03 ± 0.04
[Ti II/Fe]	0.02 ± 0.02 (2)	0.05 ± 0.02 (2)	0.03 ± 0.08 (2)	0.02 ± 0.03 (2)	0.04 ± 0.01 (2)	0.04 ± 0.01
[Cr/Fe]	0.06 ± 0.06 (10)	0.05 ± 0.06 (5)	-0.02 ± 0.03 (5)	0.04 ± 0.09 (6)	0.09 ± 0.07 (5)	0.04 ± 0.04
[Mn/Fe]	0.15 ± 0.06 (3)	0.12 ± 0.02 (4)	0.09 ± 0.01 (3)	0.25 ± 0.04 (3)	0.18 ± 0.09 (3)	0.16 ± 0.06
[Co/Fe]	0.13 ± 0.08 (4)	-0.02 ± 0.06 (6)	0.16 ± 0.06 (5)	0.26 ± 0.05 (5)	0.06 ± 0.09 (2)	0.12 ± 0.11
[Ni/Fe]	-0.02 ± 0.04 (15)	-0.03 ± 0.09 (14)	-0.05 ± 0.10 (10)	0.00 ± 0.10 (13)	0.07 ± 0.10 (18)	0.00 ± 0.05

Note: Numbers in parentheses indicate the number of lines used for the determination of abundances.

Table 3.5: Carbon, nitrogen and oxygen abundances for stars in the open cluster NGC 4815

ID	[C/H]	[C/Fe]	[N/H]	[N/Fe]	[O/H]	[O/Fe]	C/N
1795	-0.14	-0.15	0.62	0.61	0.11	0.10	0.69
358	-0.19	-0.12	0.51	0.58	0.16	0.23	0.79
210	-0.07	-0.09	0.57	0.55	0.22	0.20	0.91
95	-0.29	-0.25	0.43	0.47	-0.02	0.02	0.76
106	-0.17	-0.18	0.52	0.51	0.13	0.12	0.81
Mean	-0.17	-0.16	0.53	0.54	0.12	0.13	0.79
s.d.	± 0.08	± 0.05	± 0.07	± 0.05	± 0.09	± 0.07	± 0.08

Table 3.6: Elemental abundances for stars in the open cluster NGC 6705

ID	[C/H]	[C/Fe]	[N/H]	[N/Fe]	[O/H]	[O/Fe]	C/N
2000	−0.14	−0.09	0.57	0.62	0.04	0.09	0.78
1837	0.01	−0.06	0.74	0.67	0.27	0.20	0.74
1658	−0.12	−0.05	0.56	0.63	0.13	0.20	0.83
1625	−0.10	−0.09	0.65	0.66	0.06	0.07	0.71
1446	−0.16	−0.11	0.54	0.59	0.08	0.13	0.79
1423	0.04	−0.03	0.54	0.47	0.16	0.09	1.26
1364	−0.14	−0.16	0.53	0.51	0.07	0.05	0.85
1286	−0.12	−0.13	0.65	0.64	0.11	0.10	0.68
1256	−0.03	0.01	0.50	0.54	0.14	0.18	1.17
1248	−0.05	−0.12	0.66	0.59	0.15	0.08	0.78
1184	−0.01	0.00	0.42	0.43	0.11	0.12	1.48
1145	−0.09	−0.09	0.55	0.55	0.12	0.12	0.91
1117	−0.05	−0.11	0.66	0.6	0.14	0.08	0.78
1111	−0.07	−0.09	0.59	0.57	0.18	0.16	0.87
1090	−0.12	−0.09	0.59	0.62	0.08	0.11	0.78
963	−0.09	−0.07	0.55	0.57	0.12	0.14	0.91
916	0.03	−0.03	0.70	0.64	0.25	0.19	0.85
899	−0.04	−0.09	0.69	0.64	0.17	0.12	0.74
827	−0.16	−0.09	0.65	0.72	0.14	0.21	0.62
816	−0.17	−0.03	0.59	0.73	0.06	0.20	0.69
779	−0.08	−0.09	0.67	0.66	0.08	0.07	0.71
686	−0.10	−0.06	0.53	0.57	0.16	0.20	0.93
669	−0.05	−0.13	0.64	0.56	0.13	0.05	0.81
660	−0.08	−0.14	0.64	0.58	0.10	0.04	0.76
411	−0.06	−0.09	0.69	0.66	0.11	0.08	0.71
160	−0.12	−0.13	0.65	0.64	0.13	0.12	0.68
136	−0.10	−0.11	0.64	0.63	0.12	0.11	0.72
Mean	−0.08	-0.08	0.61	0.60	0.13	0.12	0.83
s.d.	±0.06	±0.04	±0.07	±0.07	±0.05	±0.05	±0.19

Table 3.7: Abundance results for targets in th open cluster Trumpler 20

ID	[C/H]	[C/Fe]	[N/H]	[N/Fe]	C/N
2730	−0.04	−0.22	0.46	0.28	1.26
2690	0.04	−0.17	0.60	0.39	1.10
63	−0.20	−0.20	0.39	0.39	1.02
292	−0.19	−0.21	0.43	0.41	0.95
1082	−0.11	−0.24	0.46	0.33	1.07
724	−0.17	−0.25	0.53	0.45	0.79
794	−0.24	−0.20	0.39	0.43	0.93
582	−0.02	−0.22	0.51	0.31	1.17
542	−0.01	−0.21	0.54	0.34	1.12
340	−0.18	−0.15	0.35	0.38	1.17
770	−0.08	−0.22	0.56	0.42	0.91
950	−0.09	−0.15	0.54	0.48	0.93
505	−0.11	−0.17	0.46	0.40	1.07
894	−0.09	−0.20	0.60	0.49	0.81
203	−0.09	−0.23	0.47	0.33	1.10
835	−0.10	−0.18	0.56	0.48	0.87
1010	−0.09	−0.24	0.54	0.39	0.93
923	−0.09	−0.23	0.53	0.39	0.95
858	−0.13	−0.26	0.51	0.38	0.91
227	−0.09	−0.23	0.63	0.49	0.76
346	−0.13	−0.30	0.57	0.40	0.79
781	−0.10	−0.19	0.58	0.49	0.83
768	−0.02	−0.24	0.55	0.33	1.07
791	−0.11	−0.17	0.44	0.38	1.12
287	−0.10	−0.18	0.51	0.43	0.98
1008	−0.27	−0.22	0.44	0.49	0.78
795	−0.06	−0.18	0.57	0.45	0.93
246	−0.12	−0.17	0.52	0.47	0.91
787	−0.09	−0.26	0.54	0.37	0.93
638	−0.09	−0.20	0.51	0.4	1.00

Table 3.7 – continued from previous page

ID	[C/H]	[C/Fe]	[N/H]	[N/Fe]	C/N
430	0.35	0.23	–	–	–
827	−0.09	−0.22	0.44	0.31	1.17
885	−0.08	−0.17	0.49	0.40	1.07
399	−0.06	−0.18	0.57	0.45	0.93
129	−0.10	−0.23	0.49	0.36	1.02
429	−0.11	−0.25	0.41	0.27	1.20
911	−0.22	−0.19	0.36	0.39	1.05
1044	−0.02	−0.21	0.57	0.38	1.02
591	−0.27	−0.22	0.38	0.43	0.89
468	−0.20	−0.21	0.43	0.42	0.93
679	−0.09	−0.18	0.52	0.43	0.98
3470	−0.25	−0.21	0.38	0.42	0.93
Mean	−0.10	−0.20	0.50	0.40	0.98
s.d.	±0.10	±0.07	±0.07	±0.06	±0.12

3.3 Theoretical prediction on mixing processes

Energy production in stars are driven by nucleosynthesis processes happening in the core. Afterwards the created energy is driven towards the surface by the means of convection or radiation. This energy movement creates zones of turbulence and convection inside a star, which can act as conveyor belt for chemical elements between the stars core and the surface. Heavier elements are created during the nuclear fusion happening in the center of the star, and if the convective zone reaches this layer of previously undisturbed fusion products, they are brought up to the surface. The same apply to the lighter elements (for example lithium), that get pulled down to the stellar interiors during this "dredging" event. In order to understand what drives this convection, what conditions have to be met and how they influence the abundances of chemical elements on the surface, we have to theoretically model these mixing events.

In low- and intermediate-mass stars on the main sequence the energy in the stellar

core is mainly produced during the CNO cycle through which heavier isotopes of participating elements are produced. During the first dredge up event the isotopes of ^{13}C and ^{14}N are brought up to the surface, and the ^{12}C is brought down towards the core. The effectiveness of this dredge-up depends on the mass of the metallicity of the star (Charbonnel 1994). The standard stellar evolution model considers that only convection is responsible for the 1st dredge up event. This theory also predicts that the star experiences only one such mixing event between the MS and the tip of RGB (Iben 1965), when the convective envelope deepens enough to reach the core processed material when the star enters the RGB. However it is clear that canonical models, in which convection is the only driver of mixing inside a stellar interior, explain observations of stars in the lower part of the giant branch only. Low- and intermediate-mass stars during the subsequent ascent on the RGB exhibit signatures of complex physical processes of extra-mixing that require challenging modelling. In order to describe the observed surface abundances in different types of stars, various mechanisms of extra-mixing were proposed by a number of scientific groups. In this work we compare our results with the most recent theoretical models calculated by Eggleton et al. (2008), Charbonnel & Lagarde (2010) and Lagarde et al. (2012).

3.3.1 Models of thermohaline- and rotation-induced mixing

The newest models with extra-mixing include a thermohaline instability induced mixing based on ideas of Eggleton et al. (2006) and Charbonnel & Zahn (2007). Eggleton et al. (2006) found a mean molecular weight (μ) inversion in their 1 $M_{\odot}$ stellar evolution model, occurring after the luminosity bump on the RGB, when the hydrogen burning shell reaches the chemically homogeneous part of the envelope. The μ-inversion is produced by the reaction $^{3}\mathrm{He}(^{3}\mathrm{He},2\mathrm{p})^{4}\mathrm{He}$, as predicted by Ulrich (1972). It does not occur earlier, because the magnitude of the μ-inversion is small and negligible compared to a stabilizing μ-stratification. Following Eggleton et al., Charbonnel & Zahn (2007) computed stellar models including the prescription by Ulrich (1972) and extended them to the case of a non-perfect gas for the turbulent diffusivity produced by that instability in a stellar radiative zone. They found that a double diffusive instability referred to as thermohaline convection, which had

been discussed long ago in the literature (Stern 1960), is important in the evolution of red giants. This mixing connects the convective envelope with the external wing of the hydrogen burning shell and induces surface abundance modifications in red giant stars.

Quantitative abundance values of mixing-sensitive chemical elements based on only the thermohaline mixing model have been provided by Charbonnel & Lagarde (2010). The thermohaline mixing could be an important physical process governing the surface $^{12}C/^{13}C$ and C/N ratios of stars with initial masses below 1.5 $M_{\odot}$, and its efficiency is increasing with decreasing initial stellar mass.

A decrease of $^{12}C/^{13}C$ and C/N values can also be caused by stellar rotation. Charbonnel & Lagarde (2010) computed models of rotation-induced mixing for stars at the zero-age main sequence (ZAMS) having rotational velocities of 110 km s^{-1}, 250 km s^{-1}, and 300 km s^{-1}. The convective envelope was supposed to rotate as a solid body through the evolution. The transport coefficients for chemicals associated with thermohaline- and rotation-induced mixing were simply added in the diffusion equation and the possible interactions between the two mechanisms were not considered. The rotation-induced mixing modifies the internal chemical structure of main sequence stars, although its signatures are revealed only later in the stellar evolution when the first dredge-up occurs. More recently, Lagarde et al. (2012) computed models with both the thermohaline and rotation induced mixing acting together. Lagarde et al. (2012) also assumed solid-body rotation in the convective regions, however, in addition they assumed that the transport of angular momentum is dominated by the large amount of turbulence in these regions which instantaneously flattens out the angular velocity profile as it does for the abundance profiles. The initial rotation velocity of the models on the ZAMS was chosen at 30% of the critical velocity at that point and leads to mean velocities on the main sequence between 90 and 137 km s^{-1}.

3.3.2 Comparison between the observed $^{12}C/^{13}C$ and C/N ratios and theoretical models

In figures 3.1 and 3.2 we compare the mean carbon isotope and C/N ratios of He-burning stars in different open clusters as a function of turn-off mass with the most

recent theoretical models by Eggleton et al. (2008), Charbonnel & Lagarde (2010) and Lagarde et al. (2012). We use the first dredge-up models by all three authors, and thermohaline (TH) induced mixing model by Eggleton et al. (2008) and Charbonnel & Lagarde (2010) and thermohaline- and rotation-induced mixing (TH+V) model by Lagarde et al. (2012). In addition to our results, we present the results from other authors as well. There has been a number of previous studies, however, not all of the analysed stars can be surely identified as burning helium in their cores. As we are interested in the final chemical composition changes that happen on the RGB, we have chosen to only display results of those stars, which can be attributed to being at the He-core burning phase. Results were taken from Gilroy (1989); Luck (1994); Tautvaišienė et al. (2000, 2005); Mikolaitis et al. (2010, 2011a,b, 2012); Smiljanic et al. (2009); Santrich et al. (2013).

As we can see from the presented figures, our results cover the whole range of theoretical models, however, we can group our cluster in three distinct mass intervals. Collinder 261 and Melotte 66 are the oldest clusters in our sample, with turn-off masses $< 1.5\ M_{\odot}$. The second group spans a wider range of mass values from 1.9 to around $3\ M_{\odot}$. The last group consists of two very young clusters with the largest turn-off masses $\geq 5\ M_{\odot}$.

The mean $^{12}C/^{13}C$ ratio in four clump stars of Collinder 261 is 11 ± 2 and the mean C/N ratio is equal to 1.60 ± 0.30. The mean $^{12}C/^{13}C$ and C/N ratios in red clump stars of Melotte 66 are 8 ± 2 and 1.67 ± 0.21, respectively. The turn-off mass of Collinder 261 is about $1.1\ M_{\odot}$ (Bragaglia et al. 2006) and that of Melotte 66 about $1.2\ M_{\odot}$ (Sestito et al. 2008). The average values of $^{12}C/^{13}C$ ratios in clump stars of both Collinder 261 and Melotte 66 agree well with models of extra-mixing (both thermohaline- and thermohaline+rotation-induced mixing since they are quite similar for the corresponding stellar turn-off masses of about 1.1–$1.2\ M_{\odot}$). The value of Melotte 66 is lower than that of Collinder 261 since the metallicity of this cluster is lower by about 0.5 dex. The C/N ratios are much less sensitive to mixing processes, but the figure suggests that the observational results agree with the trend of the thermohaline-induced extra-mixing model or the 1st dredge-up model (1DUP), which are very similar. The model in which the thermohaline- and rotation-induced extra-mixing act together lies lower than the observational values that were determined in our work, as well as in previous studies of open clusters.

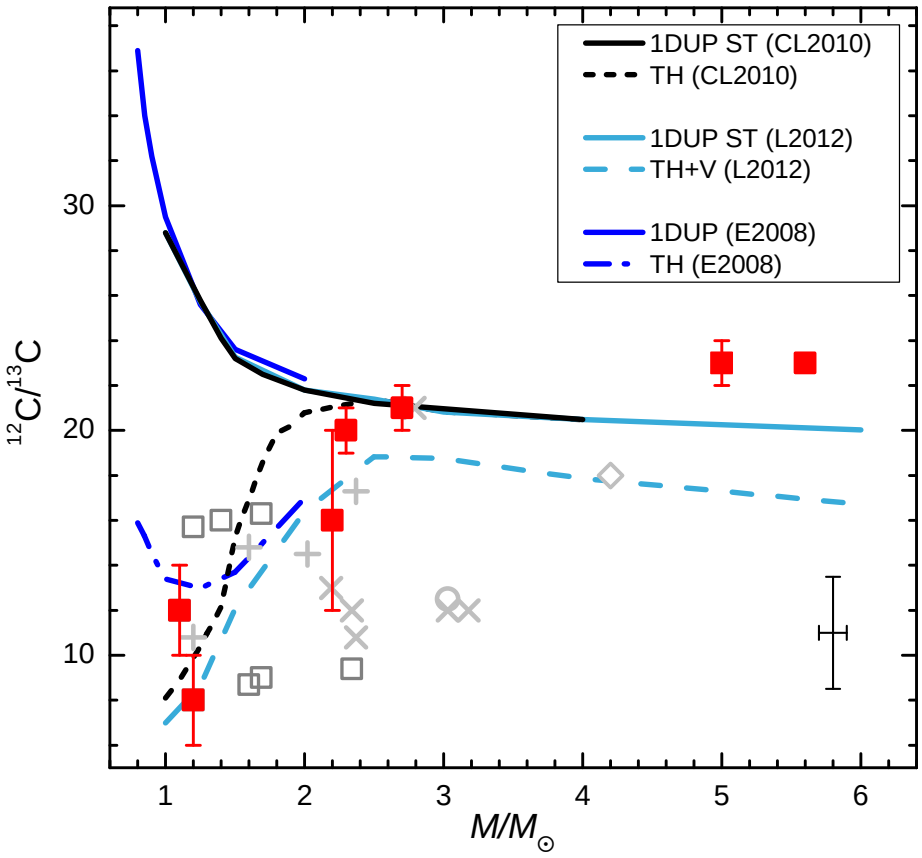

Figure 3.1: Average carbon isotope ratios in clump stars of open clusters as a function of stellar turn-off mass. The result obtained in this work are indicated by black filled squares. The previous result determined for Collinder 261 by Mikolaitis et al. (2012) is identical to ours, so they overlap. Open squares were also used to show other results from Mikolaitis et al. (2010, 2011a,b, 2012) and Tautvaišienė et al. (2000, 2005). Results from Smiljanic et al. (2009) are indicated by crosses; from Luck (1994) – open circle; from Gilroy (1989) – pluses; from Santrich et al. (2013) – open diamond. The solid lines (1DUP ST) represent the $^{12}C/^{13}C$ ratios predicted for stars at the first dredge-up with standard stellar evolutionary models of solar metallicity by Charbonnel & Lagarde (2010) (black upper line) and, more recently, Lagarde et al. 2012 (blue lower line). The black short-dashed line (TH) shows the prediction when just thermohaline extra-mixing is introduced (Charbonnel & Lagarde 2010), and the blue long-dashed line (TH+V) is for the model that includes both the thermohaline- and rotation-induced mixing (Lagarde et al. 2012). Dark blue lines indicate a theoretical model by Eggleton et al. (2008): the first dredge up model is shown as a solid blue lines, and the model with thermohaline induced mixing - as a blue dash-dot type of line. A typical error bar is indicated (Charbonnel & Lagarde 2010; Smiljanic et al. 2009; Gilroy 1989).

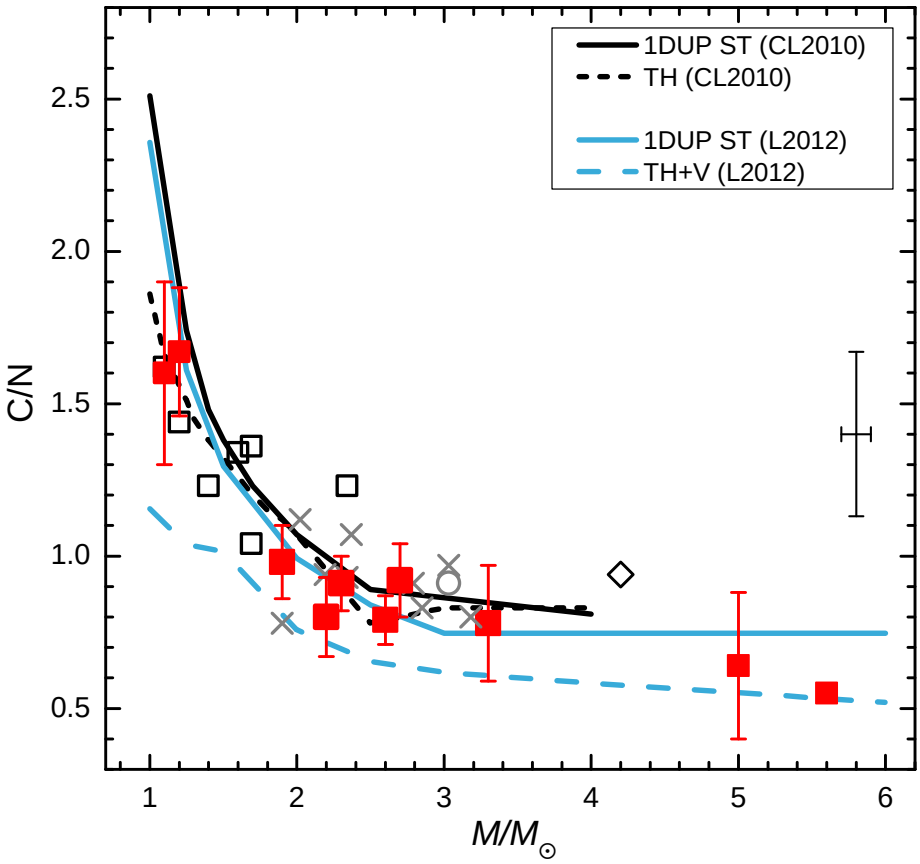

Figure 3.2: Average carbon-to-nitrogen ratios in clump stars of open clusters as a function of stellar turn-off mass. The symbols are the same as in Fig 3.1.

The turn-off mass range that was giving quite large scatter of results is around 2 $M_{\odot}$. Five of the open clusters that we analysed have a turn-off mass around this value: NGC 2324, NGC 2477, NGC 3960, NGC 4815 and Trumpler 20. The mean values of $^{12}C/^{13}C$ are 21 ± 1, 20 ± 1, and 16 ± 4 for NGC 2324, NGC 2477 and NGC 3960, respectively (NGC 4815 and Trumpler 20 had no $^{12}C/^{13}C$ ratio determination due to the lack of spectra coverage). Thus we see that the mean values of carbon isotope ratios of NGC 2324 and NGC 2477 agree well with the Charbonnel & Lagarde (2010) model of pure thermohaline-induced mixing. NGC 3960 has the lower mean carbon isotope ratio which is most probably also affected by rotation-induced mixing. The model which includes both thermohaline- and rotation-induced mixing (Lagarde et al. 2012) also gives $^{12}C/^{13}C = 16$. The rotation velocity in the model corresponds to 30% of the critical velocity at the zero-age main sequence (ZAMS, Lagarde et al. 2014, the rotation-induced mixing modifies the internal

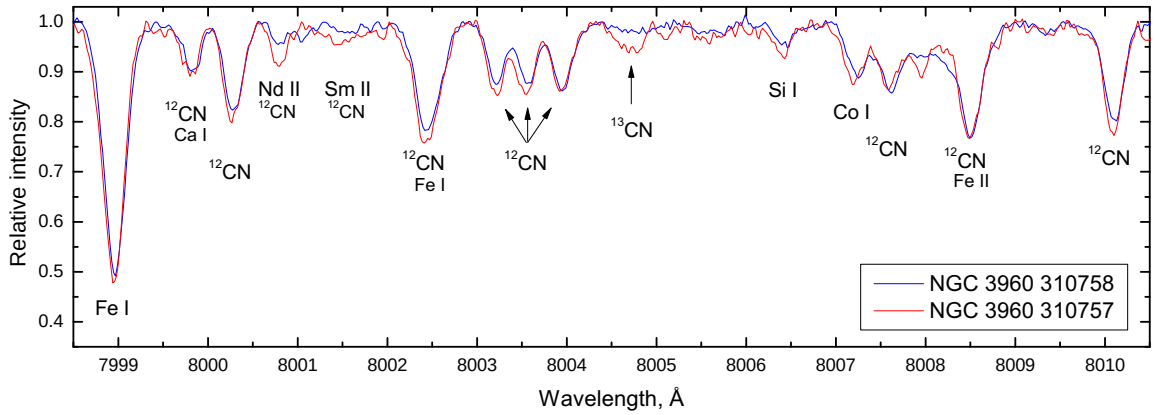

Figure 3.3: Spectra of NGC 3960 310757 (red line), which has a carbon isotope ratio equal to 10, and spectrum of NGC 3960 310758 (blue line), which has a value of 20.

chemical structure of main sequence stars, although its signatures are revealed only later in the stellar evolution). In Fig. 3.2 we see the observational results for C/N ratio for four clusters lying close to the 1DUP and thermohaline mixing models, which are very similar at these turn-off masses. The mean C/N values of NGC 2324, NGC 2477, NGC 4815 and Trumpler 20 (0.92 ± 0.12, 0.91 ± 0.20, 0.79 ± 0.08 and 0.98 ± 0.12, respectively) are close to the mentioned models. The C/N value of 0.83 ± 0.19 for the cluster NGC 6705 (turn-off mass about 3.3 $M_{\odot}$ as determined by Cantat-Gaudin et al. 2014) are very close to the values of other clusters in this mass range. So far, the model including both thermohaline- and rotation-induced mixing (Lagarde et al. 2012) predicted lower than observed C/N ratios at all turn-off masses of open clusters, however, the mean C/N ratio of NGC 3960, 0.80 ± 0.13, is comparable with this model. Maybe in the future more open clusters will be found with C/N values as low as it is predicted by this model with the ZAMS rotation velocity being 30% of the critical velocity or larger.

NGC 3960 is quite interesting. All the investigated stars are at the red clump stage with quite similar atmospheric parameters, but the $^{12}C/^{13}C$ values span from 10 to 20, and this scatter is natural. In Fig. 3.3 we compare a spectrum of NGC 3960 310757 with a carbon isotope ratio equal to 10 and a spectrum of NGC 3960 310758 with a value of 20. The difference in their ^{13}CN bands is evident.

In the the turn-off mass range larger than 4 $M_{\odot}$ we have two open clusters NGC 4609 and NGC 5316, with turn-off masses of 5.6 and 5 $M_{\odot}$, respectively. All stars in our sample are considered as being the He-core burning stars. Compared with the the-

oretical models we can see that in this mass range extra-mixing does not have a significant effect and our mean $^{12}C/^{13}C$ values agree with the standard first dredge-up and thermohaline-induced mixing model (Charbonnel & Lagarde 2010) and are not lowered as much as predicted by the models where thermohaline- and rotation-induced mixing act together (Lagarde et al. 2012). Certainly, more clusters with large TO masses should be observed in order to have a clearer picture. The same is valid in case of C/N ratios. C/N ratios have larger uncertainties, our results for both clusters are very close and seem to agree with both the first dredge-up and the thermohaline- and rotation-induced mixing models.

3.3.3 Helium flash influence on chemical mixing

In our sample of open cluster we had one, with observed stars both at the red clump position, and the star that is still climbing the RGB - the so called first ascent giants. We checked whether there is a difference in the $^{12}C/^{13}C$ ratios among these star. Our analysis indicate that the $^{12}C/^{13}C$ ratio in the first ascent giant of Collinder 261 is equal to 18 and is lower than in the more evolved clump stars that we investigated, which show the $^{12}C/^{13}C$ ratio of 12. The clump stars accumulated all chemical composition changes that took place during their evolution along the giant branch and the helium flash. Similar differences between first ascent giants, even though they lie above the RGB luminosity bump, and clump stars have been previously observed in other open clusters (M 67, Tautvaišienė et al. 2000; NGC 7789, Tautvaišienė et al. 2005; NGC 3532, Smiljanic et al. 2009; NGC 2506, Mikolaitis et al. 2011a). Collinder 261 has been analysed before as well, and we confirm the results determined by Mikolaitis et al. (2012). Their results indicate a $^{12}C/^{13}C$ ratio of 12 for red He-burning stars and 18 in the two first ascend giants which are identical to what we find.

3.3.4 Sodium abundances

Sodium is mainly produced during hydrostatic carbon burning in massive stars (Salpeter 1952; Cameron 1959) as well as in high temperature regions of H-burning during the NeNa cycle (Salpeter 1955; Denisenkov & Denisenkova 1990). Sodium can potentially be brought up to the surface when the first dredge-up occurs (El Eid

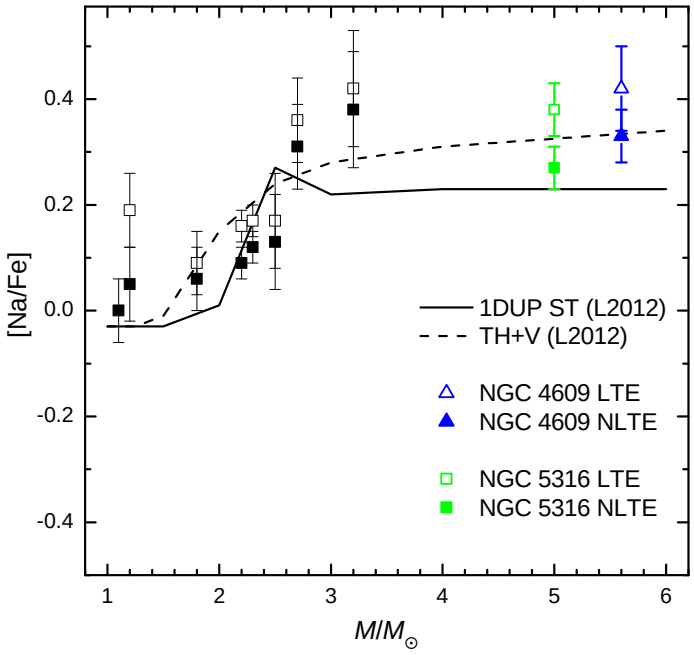

Figure 3.4: Mean [Na/Fe] values in our sample of clusters compared with theoretical extra-mixing models by Lagarde et al. (2012). Our results are indicated by green and blue symbols and results by other authors indicated as black squares (open symbols for LTE and filled squares for NLTE abundances). See text for references.

& Champagne 1995; Mowlavi 1999; Karakas 2010), however, it is not clear how effective this process might be in low- and intermediate-mass stars (Smiljanic et al. 2016 and references therein). Theoretical stellar evolution models predict that the mixing of sodium is prominent only in stars that are more massive than 1.5 - 2 $M_{\odot}$ (Charbonnel & Lagarde 2010) and especially in those that are above 4 $M_{\odot}$. More recent theoretical models, which describe chemical mixing in evolved stars (Lagarde et al. 2012), predict a significant increase (up to +0.35 dex) of sodium abundance depending on the turn-off mass.

The sodium abundances in our study were determined from three or four lines (4751.8, 5682.6, 6154.2 and 6160.8 Å). We applied non-local thermodynamic equilibrium (NLTE) corrections as described in the paper by Lind et al. (2011). The corrections range from -0.09 dex in the star NGC 5316 35 to -0.12 dex in NGC 5316 31 and NGC 5316 72. The final results for the LTE sodium abundances are [Na/Fe]=0.42 ± 0.08 for NGC 4609 and [Na/Fe]=0.38 ± 0.05 for NGC 5316. After the NLTE corrections the values were lowered to 0.33 ± 0.05 and 0.27 ± 0.04 for NGC 4609 and NGC 5316, respectively.

Smiljanic et al. (2016) in the recent study used sodium abundance results in stars of seven open clusters and compared them to chemical evolution models. However, they had open clusters with turn-off masses up to 3 $M_{\odot}$, which only allowed them to evaluate a part of the mass interval of the theoretical models. They made conclusions that the observed increase of surface sodium abundances with increasing stellar mass have to be attributed to internal evolutionary processes. In this work, we add new data points in the mass range between $5-6\ M_{\odot}$.

In Fig. 3.4 we compare mean abundances of [Na/Fe] for open clusters investigated in our study with the theoretical models. [Na/Fe] ratios for four clusters in our sample (Collinder 261, NGC 4815, NGC 6705, Trumpler 20) have been determined by Smiljanic et al. (2016). For NGC 2324, NGC 2477 and NGC 3960 we took [Na/Fe] values from Bragaglia et al. 2008, and for Melotte 66 from Sestito et al. 2008. Theoretical models by Lagarde et al. (2012) were computed for the first dredge-up and the extra-mixing which includes thermohaline- and rotation-induced mixing.

For stars with TO masses lower than $\sim 1.5\ M_{\odot}$, both models predict no change in surface sodium abundances. The results in this mass range are in agreement with models within provided error bars. For stars with masses between $1.5-3\ M_{\odot}$ even with NLTE corrections we observe the increasing overabundance of sodium in evolved stars with increasing stellar mass. Furthermore, our results of the youngest open clusters in our sample (with TO masses 5 and 5.6 $M_{\odot}$.) indicate no further increase of sodium abundances for stars heavier than $\sim 3\ M_{\odot}$.

A model of pure thermohaline-induced extra-mixing for sodium abundances was not provided by Lagarde et al. (2012), so we were not able to evaluate the agreement of observational results with this type of extra mixing as we did in the case of $^{12}C/^{13}C$ and C/N ratios. In our target clusters NGC 4609 and NGC 5316, both [Na/Fe] and C/N ratio alterations favour the model which includes thermohaline- and rotation-induced extra-mixing.

3.3.5 Oxygen abundances

While carbon and nitrogen (and sodium to some extent) abundances are susceptible to the evolutionary processes that occur inside a star, oxygen, instead, is not. The

Table 3.8: Galactocentric distances of clusters

Cluster	l deg	b deg	$d_\odot$ kpc	Ref.	$R_{\rm gc}$ kpc
Collinder 261	301.684	−05.528	2.75	1	7.0
IC 4651	340.088	−07.907	0.9	2	7.2
Melotte 66	259.559	−14.244	4.5	2	10.0
NGC 2506	230.564	09.935	3.3	1	10.4
NGC 2324	213.447	03.297	3.8	3	11.5
NGC 2477	253.563	−05.838	1.5	2	8.6
NGC 3960	294.367	06.183	2.1	4	7.4
NGC 4609	301.895	−00.142	1.3	2	7.5
NGC 4815	303.625	−02.097	2.5	5	6.9
NGC 5316	310.229	00.115	1.2	2	7.4
NGC 6134	334.917	−00.198	1.0	6	7.1
NGC 6253	335.460	−06.251	1.6	1	6.6
NGC 6705	27.307	−02.776	1.9	7	6.3

Notes. Distances from the Sun were taken from:
(1) Bragaglia & Tosi (2006), (2) Kharchenko et al. (2013), (3) Piatti et al. (2004), (4) Bragaglia et al. (2006), (5) Friel et al. (2014), (6) Ahumada et al. (2013), (7) Cantat-Gaudin et al. (2014). The $R_{\rm gc}$ values were computed with $R_{\rm gc\odot}$= 8.0 kpc.

abundances of oxygen remain more or less constant from the time a star forms and can be used to trace and study the Galactic chemical evolution.

In Fig. 3.5 we plot the determined mean oxygen abundances with respect to Galactocentric distances. We also show the theoretical models by Magrini et al. 2009 and include other observational results of open clusters that have recently been investigated by our group (Mikolaitis et al. 2010, 2011a,b, 2012; Tautvaišienė et al. 2015; Drazdauskas et al. 2016a,b). For several open clusters we recalculated the Galactocentric distances in a homogeneous way because some of the earlier determinations were based on the solar $R_{\rm gc} = 8.5$ kpc while we decided to use $R_{\rm gc\odot}$= 8.0 kpc as follows from recent studies (cf. Malkin 2013; Zhu & Shen 2013). Sources of open cluster distances from the Sun and the resulting Galactocentric distances are presented in Table 3.8. Our data points cover the $R_{\rm gc}$ from about 6 to 12 kpc.

There is a clearly visible correlation between the [O/H] abundances and the Galactocentric distance in agreement with previous studies. There are more than a few recent studies on the oxygen abundance gradients in our Galaxy related to the galac-

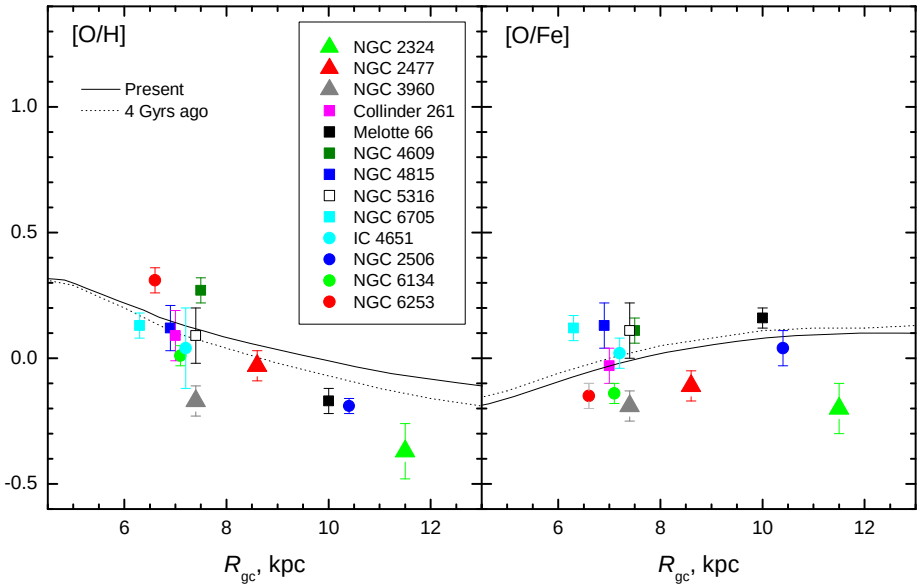

Figure 3.5: Mean oxygen abundances in relation to the Galactocentric distance compared to the theoretical models by Magrini et al. (2009). The error bars indicate the scatter of stellar abundances inside each cluster. See text for more explanations.

tocentric distance (see Magrini et al. 2009; Jacobson et al. 2009; Luck & Lambert 2011; Yong et al. 2012; Korotin et al. 2014; Martin et al. 2015; Magrini et al. 2015 and references therein). All these studies agree that there is a slight decrease in the oxygen abundance with increasing Galactocentric distance.

Some authors have suggested a bimodal distribution of the oxygen abundances (Costa et al. 2004; Magrini et al. 2009; Yong et al. 2012; Korotin et al. 2014 and references therein) with a flattening starting at around 9–13 kpc from the Galactic centre. Korotin et al. (2014), for example, suggest a double linear distribution with a slope of -0.056 dex kpc^{-1} until about $R_{\rm gc}$=12 kpc and a flatter one of -0.033 dex kpc^{-1} at more distant radii. Other authors have provided a linear fit for the oxygen abundances without any apparent changes towards the outer regions of the Galaxy. The slopes vary in different studies from -0.026 dex kpc^{-1} in Cunha et al. (2016) to -0.055 dex kpc^{-1} in Luck & Lambert (2011) or -0.06 dex kpc^{-1} in Rudolph et al. (2006). Our modest sample of open clusters supports studies with the larger slopes, but we cover only about 6 kpc, centred on the position of the Sun.

[O/Fe] trends are also under investigation. We see no apparent correlation of [O/Fe] with $R_{\rm gc}$ in our sample of clusters, which agrees with other studies. Jacobson et al. (2009) analysed the open clusters with $R_{\rm gc}$ around 10–13 kpc and concluded

that any visible trends for the [O/Fe] versus the galactocentric distance are most likely not real. Luck & Lambert (2011) found a modest increase in [O/Fe] (as well as increasing scatter) towards the outer regions of the Galaxy in Cepheids.

3.4 Final remarks

The thermohaline induced extra-mixing theory needs continuous development. For instance, in the model by Lagarde et al. (2012), the convective envelope was supposed to rotate as a solid body through the evolution, the transport coefficients for chemicals associated to thermohaline- and rotation-induced mixing were simply added in the diffusion equation and the possible interactions between the two mechanisms were not considered. Furthermore magnetic activity may also play a role. Denissenkov et al. (2009) investigated a heat exchange between rising magnetic flux rings and their surrounding medium and proposed a model of magneto-thermohaline mixing. On the basis of three-dimensional numerical simulations of thermohaline convection, Denissenkov & Merryfield (2011) suggested that the salt-finger[1] spectrum might be shifted towards larger diameters by the toroidal magnetic field. Nucci & Busso (2014) investigated magnetic advection as a mechanism for deep mixing. According to their evaluation, in this case the mixing velocities are smaller than for convection, but larger than for diffusion and adequate for extra mixing in red giants. Unfortunately, these studies have not provided values of C/N that we could compare with observations. Wachlin et al. (2011) computed full evolutionary sequences of RGB stars close to the luminosity bump and found that thermohaline mixing is not efficient enough for fingering convection to reach the bottom of the convective envelope of red giants. In order to reach the contact, the diffusion coefficient has to be artificially increased by about four orders of magnitude. Numerous shortcomings of various theoretical models was listed by Canuto (2011a,b,c,d,e). Like any new paradigm, thermohaline and other types of mixing are stimulating subsequent theoretical and observational studies.

[1]The expression "salt-finger" comes from oceanology where thermohaline mixing is also widely used to model the regions of cooler, less salty water below the warmer water where the salinity is higher because of the evaporation from the surface. The so-called "fingers" of the warmer water penetrate the cooler water and the mixing occurs when the heat excess is exchanged (e.g., Schmitt 2003; Ruddick & Kerr 2003; Kunze 2003; Radko 2010).

Chapter 4

Main results and conclusions

1. Main atmospheric parameters determined for 79 red giant stars in five open clusters (NGC 4609, NGC 4815, NGC 5316, NGC 6705, Trumpler 20). Determined carbon and nitrogen abundances for 109 red giant stars in ten open clusters, oxygen abundances for 68 red giant stars in nine open clusters, and abundance for 11 other chemical elements in the open clusters NGC 4609 and NGC 5316.

2. The mean $^{12}C/^{13}C$ and/or C/N ratios determines for ten open clusters:
   - Collinder 261 $^{12}C/^{13}C$=11$\pm$2 and C/N=1.60 $\pm$0.30 from four red clump stars, and $^{12}C/^{13}C$=18, C/N=1.74 in one first-ascent giant;
   - Melotte 66 $^{12}C/^{13}C$=8$\pm$2 as determined in four red clump stars and C/N= 1.67$\pm$0.21 derived from five red clump stars;
   - NGC 2324 $^{12}C/^{13}C$=21$\pm$1 as calculated from four red clump stars and C/N=0.92$\pm$0.12 as determined from six red clump stars;
   - NGC 2477 $^{12}C/^{13}C$=20$\pm$1 determined from four stars, and C/N= 0.91$\pm$0.09 from six stars;
   - NGC 3960 $^{12}C/^{13}C$=16$\pm$4 derived from five red clump stars and C/N= 0.80$\pm$0.13 from six red clump stars;
   - NGC 4609 $^{12}C/^{13}C$=23, C/N=0.55 derived from a single red clump star;
   - NGC 4815 C/N=0.79$\pm$0.08 as measured from five red clump stars;
   - NGC 5316 mean $^{12}C/^{13}C$=8$\pm$2 and $C/N = 0.64 \pm 0.24$ from four red clump stars;
   - NGC 6705 C/N=0.83$\pm$0.19 from 27 red giant stars;

- Trumpler 20 C/N=0.98±0.12 as determined from 42 red giant stars.

3. The determined average $^{12}C/^{13}C$ ratios in He-core burning stars for our sample of open clusters with turn-off masses $<1.5M_{\odot}$ agree well with the theoretical models which take into account thermohaline-induced mixing or with the model where both the thermohaline- and rotation-induced mixing act together. For turn-off masses $\geq 2.0\ M_{\odot}$ the mean $^{12}C/^{13}C$ values agree with the model of pure thermohaline-induced extra mixing or the first dredge up model. They are not lowered as much as predicted by the model where thermohaline- and rotation-induced mixing act together.

4. The mean C/N values for open clusters in our study with turn-off masses lower than about 3 $M_{\odot}$ agree well with the models of both the pure thermohaline-induced extra-mixing and the first dredge-up. For turn-off masses $\geq 5M_{\odot}$ the C/N ratios agree with the thermohaline- and rotation-induced mixing model, however, the results also agree within errors with the first dredge-up model.

5. The $^{12}C/^{13}C$ and C/N ratios in the investigated clump stars of NGC 3960 (turn-off mass is about 2 $M_{\odot}$) are not homogeneous. This cluster probably contains stars which are affected by the pure thermohaline-induced mixing or the first dredge-up as well as stars which are influenced by rotation-induced mixing or other extra-mixing mechanisms.

6. The mean [Na/Fe] values in the open clusters NGC 4609 and NGC 5316 indicate no further increase of sodium abundance for stars with TO masses $> 3M_{\odot}$.

7. The mean values of [O/H] agree with previous studies in exhibiting the decreasing values with increasing galactocentric distances. [O/Fe] show no apparent correlation with the $R_{\rm gc}$ in our sample of clusters.

References

Ahumada, A. V., Cignoni, M., Bragaglia, A., et al. 2013, MNRAS, 430, 221

Angelou, G. C., Stancliffe, R. J., Church, R. P., Lattanzio, J. C., & Smith, G. H. 2012, ApJ, 749, 128

Anthony-Twarog, B. J., Twarog, B. A., & McClure, R. D. 1979, ApJ, 233, 188

Asplund, M. 2004, Mem. Soc. Astron. Italiana, 75, 300

Barisevičius, G., Tautvaišienė, G., Berdyugina, S., Chorniy, Y., & Ilyin, I. 2010, Baltic Astronomy, 19, 157

Barisevičius, G., Tautvaišienė, G., Berdyugina, S., Chorniy, Y., & Ilyin, I. 2011, Baltic Astronomy, 20, 53

Battinelli, P. & Capuzzo-Dolcetta, R. 1991, MNRAS, 249, 76

Becker, W. & Fenkart, R. 1971, A&AS, 4, 241

Boothroyd, A. I. & Sackmann, I.-J. 1999, ApJ, 510, 232

Bragaglia, A., Gratton, R. G., Carretta, E., et al. 2012, A&A, 548, A122

Bragaglia, A., Sestito, P., Villanova, S., et al. 2008, A&A, 480, 79

Bragaglia, A. & Tosi, M. 2006, AJ, 131, 1544

Bragaglia, A., Tosi, M., Carretta, E., et al. 2006, MNRAS, 366, 1493

Cameron, A. G. W. 1959, ApJ, 130, 429

Cantat-Gaudin, T., Vallenari, A., Zaggia, S., et al. 2014, A&A, 569, A17

Cantiello, M. & Langer, N. 2010, A&A, 521, A9

Canuto, V. M. 2011a, A&A, 528, A76

Canuto, V. M. 2011b, A&A, 528, A77

Canuto, V. M. 2011c, A&A, 528, A78

Canuto, V. M. 2011d, A&A, 528, A79

Canuto, V. M. 2011e, A&A, 528, A80

Carraro, G., Costa, E., & Ahumada, J. A. 2010, AJ, 140, 954

Carraro, G. & Ortolani, S. 1994, A&AS, 106

Carraro, G. & Seleznev, A. F. 2012, MNRAS, 419, 3608

Carraro, G., Villanova, S., Monaco, L., et al. 2014, A&A, 562, A39

Carretta, E., Bragaglia, A., Gratton, R. G., & Tosi, M. 2005, A&A, 441, 131

Chanamé, J., Pinsonneault, M., & Terndrup, D. M. 2005, ApJ, 631, 540

Charbonnel, C. 1994, A&A, 282, 811

Charbonnel, C. 2006, in EAS Publications Series, Vol. 19, EAS Publications Series, ed. T. Montmerle & C. Kahane, 125–146

Charbonnel, C. & Lagarde, N. 2010, A&A, 522, A10

Charbonnel, C. & Zahn, J.-P. 2007, A&A, 467, L15

Chen, L., Hou, J. L., & Wang, J. J. 2003, AJ, 125, 1397

Claria, J. J., Lapasset, E., & Minniti, D. 1989, A&AS, 78, 363

Costa, R. D. D., Uchida, M. M. M., & Maciel, W. J. 2004, A&A, 423, 199

Cuffey, J. 1941, ApJ, 94, 55

Dawson, D. W. 1978, AJ, 83, 1424

De Silva, G. M., Freeman, K. C., Asplund, M., et al. 2007, AJ, 133, 1161

Dekker, H., D'Odorico, S., Kaufer, A., Delabre, B., & Kotzlowski, H. 2000, in Proc. SPIE, Vol. 4008, Optical and IR Telescope Instrumentation and Detectors, ed. M. Iye & A. F. Moorwood, 534–545

Denisenkov, P. A. & Denisenkova, S. N. 1990, Soviet Astronomy Letters, 16, 275

Denissenkov, P. A. 2010, ApJ, 723, 563

Denissenkov, P. A. & Merryfield, W. J. 2011, ApJ, 727, L8

Denissenkov, P. A., Pinsonneault, M., & MacGregor, K. B. 2009, ApJ, 696, 1823

Donati, P., Cantat Gaudin, T., Bragaglia, A., et al. 2014, A&A, 561, A94

Drazdauskas, A., Tautvaišienė, G., Randich, S., et al. 2016a, A&A, 589, A50

Drazdauskas, A., Tautvaišienė, G., Smiljanic, R., Bagdonas, V., & Chorniy, Y. 2016b, MNRAS, 462, 794

Eggen, O. J. & Stoy, R. H. 1961, Royal Greenwich Observatory Bulletins, 24

Eggen, O. J. & Stoy, R. H. 1962, Royal Greenwich Observatory Bulletins, 53, 7

Eggleton, P. P., Dearborn, D. S. P., & Lattanzio, J. C. 2006, Science, 314, 1580

Eggleton, P. P., Dearborn, D. S. P., & Lattanzio, J. C. 2008, ApJ, 677, 581

El Eid, M. F. & Champagne, A. E. 1995, ApJ, 451, 298

Feinstein, A. & Marraco, H. G. 1971, PASP, 83, 218

Friel, E. D. 1995, ARA&A, 33, 381

Friel, E. D., Donati, P., Bragaglia, A., et al. 2014, A&A, 563, A117

Friel, E. D., Jacobson, H. R., Barrett, E., et al. 2003, AJ, 126, 2372

Friel, E. D. & Janes, K. A. 1993, A&A, 267, 75

Friel, E. D., Janes, K. A., Tavarez, M., et al. 2002, AJ, 124, 2693

Frinchaboy, P. M. & Majewski, S. R. 2008, AJ, 136, 118

Geisler, D., Claria, J. J., & Minniti, D. 1992, AJ, 104, 1892

Geisler, D. P. & Smith, V. V. 1984, PASP, 96, 871

Gilroy, K. K. 1989, ApJ, 347, 835

Gilroy, K. K. & Brown, J. A. 1991, ApJ, 371, 578

Gonzalez, G., Lambert, D. L., Wallerstein, G., et al. 1998, ApJS, 114, 133

Gonzalez, G. & Wallerstein, G. 2000, AJ, 119, 1839

Gozzoli, E., Tosi, M., Marconi, G., & Bragaglia, A. 1996, MNRAS, 283, 66

Gratton, R., Bragaglia, A., Carretta, E., & Tosi, M. 2006, ApJ, 642, 462

Gratton, R. G. 1982, ApJ, 257, 640

Gratton, R. G., Carretta, E., Eriksson, K., & Gustafsson, B. 1999, A&A, 350, 955

Gratton, R. G. & Contarini, G. 1994, A&A, 283, 911

Gratton, R. G., Sneden, C., Carretta, E., & Bragaglia, A. 2000, A&A, 354, 169

Grevesse, N., Asplund, M., & Sauval, A. J. 2007, Space Sci. Rev., 130, 105

Gurtovenko, E. A. & Kostyk, R. I. 1989, Kiev Izdatel Naukova Dumka

Gustafsson, B., Edvardsson, B., Eriksson, K., et al. 2008, A&A, 486, 951

Hartwick, F. D. A., Hesser, J. E., & McClure, R. D. 1972, ApJ, 174, 557

Hawarden, T. G. 1976, MNRAS, 174, 471

Heiter, U., Soubiran, C., Netopil, M., & Paunzen, E. 2014, A&A, 561, A93

Hou, J.-L., Chang, R.-X., & Chen, L. 2002, Chinese J. Astron. Astrophys., 2, 17

Iben, Jr., I. 1965, ApJ, 142, 1447

Iben, Jr., I. 1967, ApJ, 147, 624

Jacobson, H. R., Friel, E. D., & Pilachowski, C. A. 2009, AJ, 137, 4753

Janes, K. & Adler, D. 1982, ApJS, 49, 425

Janes, K. A. 1981, AJ, 86, 1210

Johansson, S., Litzén, U., Lundberg, H., & Zhang, Z. 2003, ApJ, 584, L107

Johnson, H. L., Sandage, A. R., & Wahlquist, H. D. 1956, ApJ, 124, 81

Jura, M. 1987, ApJ, 313, 743

Karakas, A. I. 2010, MNRAS, 403, 1413

Kassis, M., Janes, K. A., Friel, E. D., & Phelps, R. L. 1997, AJ, 113, 1723

Kharchenko, N. V., Piskunov, A. E., Schilbach, E., Röser, S., & Scholz, R.-D. 2013, A&A, 558, A53

King, I. R. 1964, Royal Greenwich Observatory Bulletins, 82, 106

Kjeldsen, H. & Frandsen, S. 1991, A&AS, 87, 119

Koo, J.-R., Kim, S.-L., Rey, S.-C., et al. 2007, PASP, 119, 1233

Korotin, S. A., Andrievsky, S. M., Luck, R. E., et al. 2014, MNRAS, 444, 3301

Kunze, E. 2003, Progress in Oceanography, 56, 399

Kupka, F. G., Ryabchikova, T. A., Piskunov, N. E., Stempels, H. C., & Weiss, W. W. 2000, Baltic Astronomy, 9, 590

Kurucz, R. L. 2005, Memorie della Societa Astronomica Italiana Supplementi, 8, 189

Kyeong, J.-M., Byun, Y.-I., & Sung, E.-C. 2001, Journal of Korean Astronomical Society, 34, 143

Lada, C. J. & Lada, E. A. 2003, ARA&A, 41, 57

Lagarde, N., Charbonnel, C., Decressin, T., & Hagelberg, J. 2011, A&A, 536, A28

Lagarde, N., Decressin, T., Charbonnel, C., et al. 2012, A&A, 543, A108

Lattanzio, J. C., Siess, L., Church, R. P., et al. 2015, MNRAS, 446, 2673

Lind, K., Asplund, M., Barklem, P. S., & Belyaev, A. K. 2011, A&A, 528, A103

Lindoff, U. 1968, Arkiv for Astronomi, 5, 1

Luck, R. E. 1994, ApJS, 91, 309

Luck, R. E. & Lambert, D. L. 2011, AJ, 142, 136

Magrini, L., Randich, S., Donati, P., et al. 2015, A&A, 580, A85

Magrini, L., Sestito, P., Randich, S., & Galli, D. 2009, A&A, 494, 95

Malkin, Z. 2013, in IAU Symposium, Vol. 289, Advancing the Physics of Cosmic Distances, ed. R. de Grijs, 406–409

Martin, R. P., Andrievsky, S. M., Kovtyukh, V. V., et al. 2015, MNRAS, 449, 4071

Mathieu, R. D., Latham, D. W., Griffin, R. F., & Gunn, J. E. 1986, AJ, 92, 1100

Mazur, B., Krzeminski, W., & Kaluzny, J. 1995, MNRAS, 273, 59

McNamara, B. J., Pratt, N. M., & Sanders, W. L. 1977, A&AS, 27, 117

McSwain, M. V. & Gies, D. R. 2005, ApJS, 161, 118

Mermilliod, J. C. 1981, A&AS, 44, 467

Mermilliod, J. C., Mayor, M., & Udry, S. 2008, A&A, 485, 303

Messina, S., Parihar, P., Koo, J.-R., et al. 2010, A&A, 513, A29

Mikolaitis, Š., Tautvaišienė, G., Gratton, R., Bragaglia, A., & Carretta, E. 2010, MNRAS, 407, 1866

Mikolaitis, Š., Tautvaišienė, G., Gratton, R., Bragaglia, A., & Carretta, E. 2011a, MNRAS, 413, 2199

Mikolaitis, Š., Tautvaišienė, G., Gratton, R., Bragaglia, A., & Carretta, E. 2011b, MNRAS, 416, 1092

Mikolaitis, Š., Tautvaišienė, G., Gratton, R., Bragaglia, A., & Carretta, E. 2012, A&A, 541, A137

Moffat, A. F. J. & Vogt, N. 1973, A&AS, 10, 135

Mowlavi, N. 1999, A&A, 350, 73

Nucci, M. C. & Busso, M. 2014, ApJ, 787, 141

Origlia, L., Valenti, E., Rich, R. M., & Ferraro, F. R. 2006, ApJ, 646, 499

Pallavicini, R. 2003, Memorie della Societa Astronomica Italiana Supplementi, 3, 74

Pasquini, L., Avila, G., Blecha, A., et al. 2002, The Messenger, 110, 1

Pereira, T. M. D., Kiselman, D., & Asplund, M. 2009, A&A, 507, 417

Phelps, R. L., Janes, K. A., & Montgomery, K. A. 1994, AJ, 107, 1079

Piatti, A. E., Claria, J. J., & Abadi, M. G. 1995, AJ, 110, 2813

Piatti, A. E., Clariá, J. J., & Ahumada, A. V. 2004, A&A, 418, 979

Piatti, A. E., Clariá, J. J., Bica, E., Geisler, D., & Minniti, D. 1998, AJ, 116, 801

Platais, I., Melo, C., Fulbright, J. P., et al. 2008, MNRAS, 391, 1482

Prisinzano, L., Carraro, G., Piotto, G., et al. 2001, A&A, 369, 851

Prisinzano, L., Micela, G., Sciortino, S., & Favata, F. 2004, A&A, 417, 945

Radko, T. 2010, Journal of Fluid Mechanics, 645, 121

Ruddick, B. & Kerr, O. 2003, Progress in Oceanography, 56, 483

Rudolph, A. L., Fich, M., Bell, G. R., et al. 2006, ApJS, 162, 346

Sacco, G. G., Morbidelli, L., Franciosini, E., et al. 2014, A&A, 565, A113

Salpeter, E. E. 1952, ApJ, 115, 326

Salpeter, E. E. 1955, Physical Review, 97, 1237

Santos, Jr., J. F. C., Bonatto, C., & Bica, E. 2005, A&A, 442, 201

Santrich, O. J. K., Pereira, C. B., & Drake, N. A. 2013, A&A, 554, A2

Schmitt, R. W. 2003, Progress in Oceanography, 56, 419

Seleznev, A. F., Carraro, G., Costa, E., & Loktin, A. V. 2010, New A, 15, 61

Sestito, P., Bragaglia, A., Randich, S., et al. 2006, A&A, 458, 121

Sestito, P., Bragaglia, A., Randich, S., et al. 2008, A&A, 488, 943

Smiljanic, R., Gauderon, R., North, P., et al. 2009, A&A, 502, 267

Smiljanic, R., Korn, A. J., Bergemann, M., et al. 2014, A&A, 570, A122

Smiljanic, R., Romano, D., Bragaglia, A., et al. 2016, ArXiv e-prints

Sneden, C. & Pilachowski, C. A. 1986, ApJ, 301, 860

Stern, M. E. 1960, Tellus, 12, 172

Stetson, P. B. & Pancino, E. 2008, PASP, 120, 1332

Sung, H., Bessell, M. S., Lee, H.-W., Kang, Y. H., & Lee, S.-W. 1999, MNRAS, 310, 982

Tautvaišienė, G., Drazdauskas, A., Mikolaitis, Š., et al. 2015, A&A, 573, A55

Tautvaišienė, G., Edvardsson, B., Puzeras, E., Barisevičius, G., & Ilyin, I. 2010, MNRAS, 409, 1213

Tautvaišienė, G., Edvardsson, B., Puzeras, E., & Ilyin, I. 2005, A&A, 431, 933

Tautvaišienė, G., Edvardsson, B., Tuominen, I., & Ilyin, I. 2000, A&A, 360, 499

Tautvaišienė, G., Edvardsson, B., Tuominen, I., & Ilyin, I. 2001, A&A, 380, 578

Tautvaišienė, G. & Puzeras, E. 2009, in IAU Symposium, Vol. 254, The Galaxy Disk in Cosmological Context, ed. J. Andersen, Nordströara, B. m, & J. Bland-Hawthorn, 75

Twarog, B. A., Ashman, K. M., & Anthony-Twarog, B. J. 1997, AJ, 114, 2556

Twarog, B. A., Twarog, B. J. A., & Hawarden, T. G. 1995, PASP, 107, 1215

Ulrich, R. K. 1972, ApJ, 172, 165

Škoda, P., Draper, P. W., Neves, M. C., Andrešič, D., & Jenness, T. 2014, Astronomy and Computing, 7, 108

van den Bergh, S. & Hagen, G. L. 1975, AJ, 80, 11

Wachlin, F. C., Miller Bertolami, M. M., & Althaus, L. G. 2011, A&A, 533, A139

Yong, D., Carney, B. W., & Friel, E. D. 2012, AJ, 144, 95

Zhu, Z. & Shen, M. 2013, in IAU Symposium, Vol. 289, Advancing the Physics of Cosmic Distances, ed. R. de Grijs, 444–447

Acknowledgements

First of all I wish to express my gratitude to my supervisor Gražina Tautvaišienė for leading me through all the study process, encouragement and support. I am thankful to all my collaborators and especially to Sofia Randich, Angela Bragaglia, Rodolfo Smiljanic and the Gaia-ESO consortium for the valuable observational data. Bertrand Plez (University of Montpellier II) and Guillermo Gonzalez (Washington State University) were particularly generous in providing us with atomic data for CN and C_2 molecules, respectively. I would like to thank Erasmus+ for the provided opportunity to visit the Observatoire de la Côte d'Azur in Nice (France) and the valuable experience i gained during my stay there. This research has made use of SIMBAD (operated at CDS, Strasbourg, France), VALD (Kupka et al. 2000) and NASA's Astrophysics Data System. I thank the referees of all papers and this thesis for a careful reading of the manuscript and constructive suggestions for the improvement of the work. This research was partially funded by the grant from the Research Council of Lithuania (MIP-082/2015).